Universiteit Utrecht

Bachelor Thesis

Understanding the X-ray absorption and emission in archetypal radio-loud AGN 3C 273 with XMM-Newton RGS

Nejc Blaznik
5713625

Supervisor
Missagh Mehdipour
Netherlands Institute for Space Research (SRON)

Spring Summer - 2018

Understanding the X-ray absorption and emission in archetypal radio-loud AGN 3C 273 with XMM-Newton RGS

Nejc Blaznik

Supervisor: M. Mehdipour

June 2018

Contents

List of Figures

List of Tables

Abstract

In this thesis I present the results from high-resolution X-ray spectroscopic observations in the direction of Seyfert Type-1 AGN 3C 273, using RGS detectors mounted on *XMM-Newton*. AGNs are currently one of the most investigated objects in the universe. With the recent progress done in X-ray observations, mostly thanks to high resolution *Chandra* and *XMM-Newton* observatories, many questions could now be answered or addressed from a different perspective. Nonetheless, there is still a large number of questions to which this thesis, and many other papers will try to find an answer to. Using the observations, the recorded spectrum from 6 to 38 Å was analysed with several models for fitting the continuum and distinct absorption and emission lines, provided by `SPEX` software package. We show that power-law ($\Gamma = 1.54 \pm 0.01$) describes the basic continuum model sufficiently, and is further improved by using 'warm' Comptonisation ($T \approx 1.8$ keV) to model the soft X-ray excess. We identify several gas absorption lines occurring in three different components of Milky Way gas, at temperatures approximately 0.5 eV, 10 ev, and 130 eV, with varying velocities between -100 km/s and 500 km/s, which is in agreement with the results obtained in previous studies of the source. We also identify broad emission lines of O VII and Ne IX triplet, as well as O VIII Lyman-α emissions in broad line region (BLR) of the AGN. We investigate the possibility of photoionised plasma absorption lines from the AGN wind, but can only determine an upper limit of the N_H. This limit is relatively low, $N_H = 1.9^{+2}_{-1} \times 10^{22}$ m^{-2}, and therefore does not substantially improve the fit to the spectrum, which suggest that there is no significant wind present in this radio-loud AGN.

Chapter 1

Introduction

1.1 Active Galactic Nuclei

Active galactic nucleus (AGN) is a name assigned to the central region of an active galaxy, which is brighter than normal in luminosity over most parts of - and very often over the whole - electromagnetic spectrum. The most luminous of the AGNs have a specific name: *quasars*. The name comes from *quasi-stellar radio source*, which is how those object were originally observed. They appeared star-liked when observed from the Earth, but their red-shift indicated that they were much further away than any observed star. Their immense luminosities are what enables us to investigate their properties. It is a widely accepted theory, that their brightness originates from accretion of gas onto the supermassive black hole (SMBH), found in the centre of every AGN. The inflows of matter (gasses) towards the black hole are usually accompanied by outflows of matter and energy in the form of winds of ionised gas, and in some cases powerful collimated jets of matter of lengths of hundreds of thousands light years, moving at relativistic velocities. The energy emitted by quasars, which usually ranges between 10^{36} and 10^{41} W, can be detected at different wavelengths, from low energetic radio waves (high wavelengths) to high energetic X-rays (small wavelengths).

Over the years, a collection of observational data and progressively more complex X-ray astronomy missions, such as *Chandra* and *XMM-Newton* observatories launched in 1999, led to the formulation of a *Unified Model* of AGNs. The model states, that the differences in observed properties of AGNs, and different names assigned to them, can in most cases be explained by different *viewing angles* of the observer. Even though this model is widely used in the astronomical community, it is still not completely clear whether it can explain all the observed differences between different types of AGNs (Pradhan and Nahar, 2011). The model states that the central SMBH and its accretion disc are surrounded by an optically thick torus, made of molecular gas and dust, which is heated by the radiation from the accretion disc. Clouds within the torus and above the disk then reprocesses the emission from the disc into the broad optical and UV emission lines, while the heated gas clouds outside the torus give rise to narrow optical and UV emission lines. The region where the former happens is known as broad line region (BLR), and the latter is known as the narrow line region (NLR). Based on the type of lines observed, which will depend

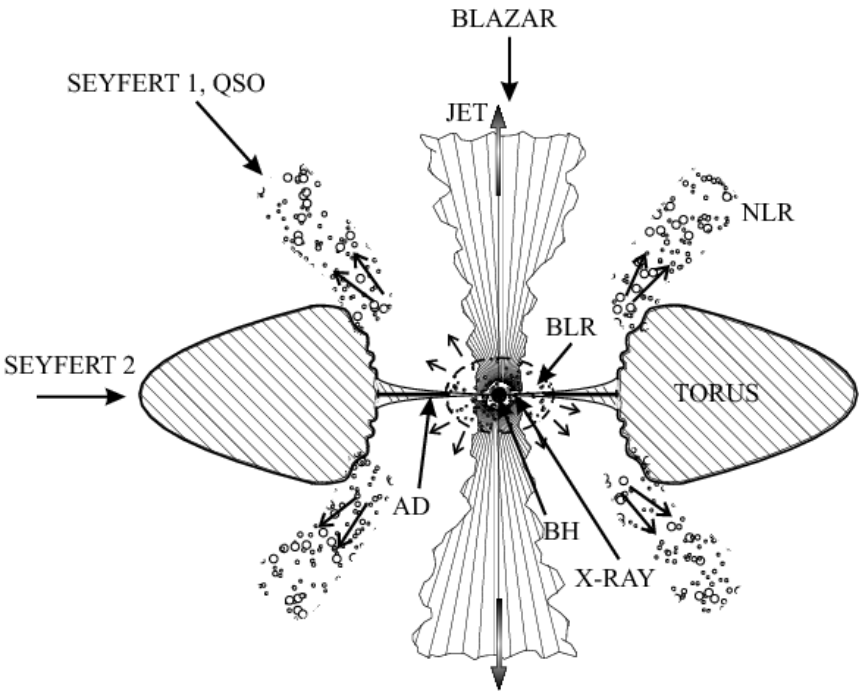

Figure 1.1: A sketch of a typical radio-loud AGN. It can be noticed, that if the AGN is observed along different directions, the observed emission and absorption will be dominated by different parts of the AGN. The abbreviations stand for accretion disc (AD), black hole (BH) broad line region (BLR), narrow line region (NLR), quasi-stellar object (QSO). Credit: Jovanović and Popović (2009)

on our viewing angle, different types of galaxies can be identified (see figure 1.1). If we are looking directly down the jet, the AGN is called blazar, and the observed emission will be dominated by the phenomena occurring in the jet. Observed emission lines will in this case differ from an AGN observed side-on, called a Type-2 AGN, or Seyfert-2 AGN. The intermediate step between a blazar and a Seyfert-2 AGN is a Seyfert-1 AGN. If the emission lines from both BLR and NLR will be visible, then the viewer's line of the central region is not obscured by the torus, and we are talking about the Type-1 AGN. If our view is side-on, the central region and the BLR clouds are hidden, and we are talking about the Type-2 AGN. If in the AGN the jets of plasma emitted from the nucleus are present, we call such AGN *radio-loud*, if not, *radio-quiet*. The AGN investigated in this thesis, 3C 273, is a Seyfert-1 type of radio-loud AGN, also known as a *broad-line radio galaxy* (BLRG).

1.2 Theoretical background

1.2.1 Absorption and emission of X-rays

Two of the main concepts of this essay are the processes of absorption and emission. As the names suggest, in the case of absorption an atom/ion absorbs a photon, and in doing so it gains the energy previously carried by the photon, $E_\gamma = h\nu$, and an electron 'jumps' to a higher energy level. The emission process is the reverse of that - an excited atom/ion emits a photon, and in doing so an electron 'falls' down to a lower energy level, and thus the energy of the newly emitted photon, $E_e - E_g = h\nu$. If the photon hitting an atom has enough energy to completely remove an electron from its shell, the atom will undergo *ionisation*, and the excess energy from the photon will be used to increase the atom's kinetic energy (i.e. temperature). In the case that this incoming energy needed for removing an electron comes from a highly energetic photon (e.g. X-ray), such process is called *photoionisation*. A common way of referring to an ionisation state of a given element in a spectrum is by using the symbol of an element, followed by a Roman numeral. By convention, Roman numeral I is associated with the absorption or emission lines produced by a neutral element (no electrons were removed from the element), Roman numeral II indicates that 1 electron was removed from the element, III that 2 electrons were removed and so on. If an element was ionised many times and only one or two electrons are remaining, we call such elements hydrogen or helium like, respectively.

Even though the explanation of the very process that gives rise to the emission of the X-rays in AGNs is still controversial (e.g. Uchiyama et al. (2006)), it is commonly acknowledged that the mechanism responsible for emission of X-rays in the AGN is the presence of a hot medium, which emits the radiation of higher energies. It is believed that this medium is a hot corona of highly energetic electrons located near the accretion disc, which can up-scatter photons that lie in lower energy UV/optical bands, into more energetic X-ray band. This process is called *inverse Comptonisation*, and offers a solution to the observed power-law shape of the continuum in the X-ray band. Apart from the power-law component of the X-ray continuum of AGN, another component is needed for a better fit - the *soft X-ray excess*. At lower energies, the spectrum is observed to be slightly steepened above the extrapolated X-ray power-law. This property has been observed in the majority of all observed AGNs, however the mechanism behind is still an active field of research (see e.g. Done et al. (2012)) (see section 2.2).

1.2.2 AGN winds

Observations show that supermassive black holes play an important role on the evolution of their host galaxies, and vice versa (e.g. Ferrarese and Merritt (2000)). The outflows from the AGN may play a significant role in this relation, as they can impact the environment and the star formation in the galaxy (e.g. Silk and Rees (1998)). One of the essential parts of the outflows in AGNs are winds of photoionised gas, also called warm absorbers. They imprint their absorption lines on the continuum, making it an important part of the spectrum. Since the launch of *XMM-Newton* and *Chandra* many new insights into the structure of these winds has been made, such as investigating wind's

ionisation and velocity components (e.g. Crenshaw et al. (1999)), and column densities (e.g. Mehdipour et al. (2015a)). Nevertheless, there still remains many open questions concerning winds, in particular their origin, their impact on the environment, and their launching mechanisms. As the outflows ultimately arise due to the energy released form the accretion processes, it is expected that their properties will in many ways reflect the physical conditions of the accretion disk. However, it is still not clear which processes and factors exactly govern the launch of those outflows. One of the suggested explanations is that the ionised outflows could be AGN winds, thermally-driven from the torus (e.g. Krolik and Kriss (2001)), or that they result as magnetohydrodynamic (e.g. Fukumura et al. (2010)) or radiatively-driven (e.g. Proga et al. (2000)) winds from the accretion disk. In particular the existence of ionised winds in radio-loud AGN with powerful winds is rather uncertain, and poorly understood.

1.2.3 Hot gas in the Milky Way

Similarly as in the case of AGN and its winds, the hot interstellar medium (ISM) in the Galaxy[1] plays an important role in stellar feedback and regulation of the Galaxy's ecosystem. Nevertheless, the origin of this hot gas in Milky Way is still not fully understood. Since the path of radiation from 3C 273 (located at the Galactic coordinates: longitude $l = 289.951°$, latitude $b = 64.360°$, (Johnston et al., 1995)) to the observatories in the Earth's orbit passes through Galactic ISM (see figure 1.2), it is important to take it into account when investigating the absorption and emission lines. In particular, we will try to determine whether the absorption and emission lines seen in the spectrum are due to the processes happening at 3C 273, or in the ISM of the Milky Way. Due to the expansion of the Universe, we can expect the lines from the AGN to be red-shifted, which will help us to distinguish between AGN and Milky Way lines. Based on the angles and the numerical data available for the lowest limit of the thickness of the disk of ISM ($\approx$ 0.6 kpc (Rix and Bovy, 2013)), and assuming that the earth lies relatively close to the Galactic plane ($\pm \sim$ 20 pc (Blaauw et al., 1960)), we can estimate that the distance that the radiation travels through the parts of Milky Way where absorption and emission happen is of few kpc (as also confirmed by Marasco et al. (2013), which is about a 10^{-6} part of the entire distance to 3C 273. Many papers cite this number to be of many orders of magnitude larger, taking into account that the hot absorbing gas can kinetically be found up to few Mpc around the Galaxy (e.g. Wang (2009)). Since we expect the ratio of column density of the ISM in the Milky Way compared to the density of the intergalactic medium (IGM) to be much bigger, namely in the orders of $\sim 10^{11}$, it is safe to assume that the Milky Way absorptions will play a much bigger role than random absorption processes happening in the IGM.

With the progress in the last two decades in X-ray absorption and emission high-resolution spectroscopy (*Chandra, XMM-Newton*, and *Suzaku* (Mitsuda et al., 2007)), the hot ISM in the Milky Way has become further understood - in particular its global spatial, chemical, thermal and kinematic properties (e.g. Nakanishi and Sofue (2003)).

[1]We will take use of a convention that the word 'Galaxy' when written with a capital 'G' refers to the Milky Way

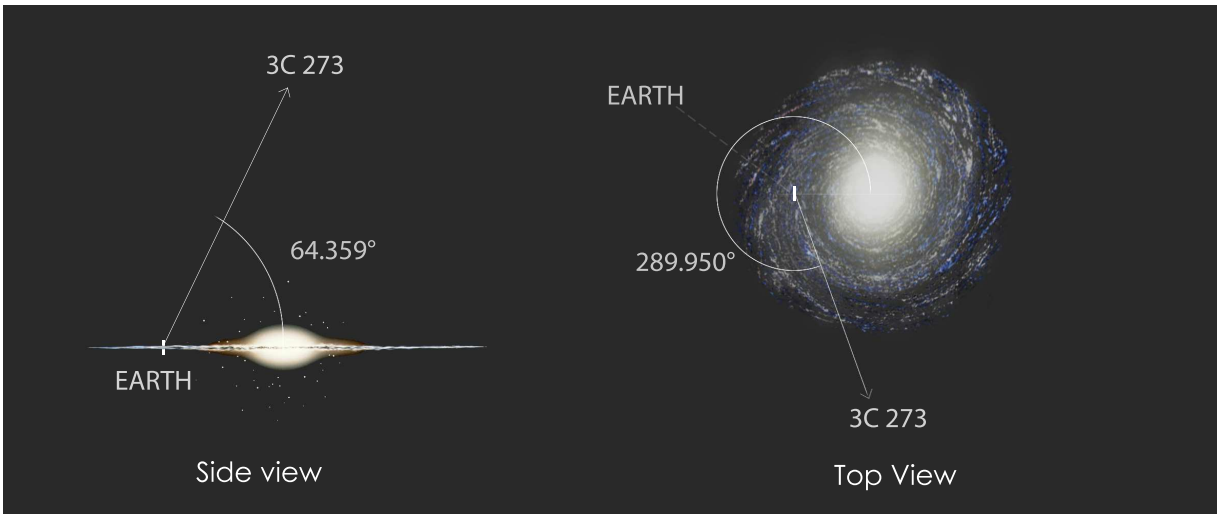

Figure 1.2: The direction to 3C 273 from Earth. Indicated are the numerical values for the angles of the galactic coordinate longitude and latitude. The pictures and distances are only symbolic and not to scale (3C 273 is almost 10^8 times further from us than the centre of the galaxy, Sagittarius A*). Credit: numerical factors from Johnston et al. (1995), pictures from J. Baum & N. Henbest, edited and labelled by myself.

The results are more or less consistent with the X-ray imaging of nearby similar galaxies (Wang, 2009). Typical temperatures of the hot ISM gas are around $\sim 10^6$ K, with the presence of hotter, lower density clouds (which result in characteristic absorptions for high-velocity clouds) not excluded from the model. The observed emission spectrum shows O VII, O VIII, and Ne IX Kα lines, which strongly suggests the presence of hot optically thin thermal plasma, with $T \sim 2.4 \times 10^6$ K (Wang et al., 2005). Similarly, thanks to *Chandra* and *XMM-Newton*, global-hot-gas absorption lines give us direct insight into ISM ions' column densities, which in turn give us the information about the the mass of the gas, and its kinematic, chemical and thermal properties.

Hot gas can serve as an enormous reservoir for stellar formation. Just in Milky Way, with the current rate of stellar production it would take few Gyr to completely use up all the material (Diehl et al., 2006). The star formation rate however only decreased by a factor of 2-3 in the last few Gyr, which implies that the ISM gets continuously replenished (Fraternali and Tomassetti, 2012). The main candidate explaining this phenomena is the accretion from cosmological coronae (Marasco et al., 2013). There are several different proposed mechanisms that be responsible for the heating up of the gas to high temperatures, operating at different spatial scales, such as the dark matter potential well induced accretion shock ($\approx$ 250 kpc in the Milky Way), and outflows driven by the supernova closer to the disk ($\approx$ 10 kpc) (Miller et al., 2016).

Since the angle of the sight-line towards the 3C 273 is pointing towards the inner parts of the Galaxy, (figure 1.2), another phenomenon needs to be mentioned and taken into

consideration. It has been noticed that towards the inner parts of the Galaxy, a general enhancement is shown in the X-ray background between 0.5-2 keV (e.g. Wang (2009)). The enhancement results in significantly different thermal and kinematic properties of the gas. By studying bright AGNs with similar Galactic latitudes but facing off the enhancement, such as Mrk 421, it is possible to subtract the combined foreground and background contribution, and determine the net X-ray absorption and emission resulting from the enhancement towards the 3C 273 (Yao and Wang, 2007). Analysis show that the average temperature of the hot gas in this direction is 2×10^6 K, and its dispersion velocity 216 km s^{-1}, which differ significantly for measurements done in the direction opposite to the enhancement. The very nature of this enhancement is still a subject of discussion, but it is probably a result of a combination of the outflow from the Galactic nucleus, and a nearby superbubble. Away from this enhanced inner region, the Galactic disk contribution is quite uniform. The Galactic disk contribution represents the hot ISM as well as the contribution from the stellar emission.

1.3 Extremely powerful quasar 3C 273

In this thesis, the main focus will lie on the spectroscopy of the object in the constellation of Virgo, characterised as the 273rd object of the Third Cambridge Catalogue of Radio Sources (3C), or known simply as 3C 273. 3C 273 was the first identified quasar, when in 1963, Maarten Schmidt recognised several of its well-known broad emission lines, which had an unusually large red-shift for such a bright object (Schmidt, 1963). This placed the object much further away from the Earth than originally postulated. The latest calculated value of red-shift for 3C273 is

$$z = 0.158339[0.000067], (\text{Strauss et al., 1992}),$$

or approximately 2 billion light-years. This quasar is also the brightest one in the sky - its absolute magnitude of about -26.7 (Greenstein and Schmidt, 1964), and average apparent magnitude of $m \sim 12,8$ (obtained from NASA/IPAC EXTRAGALACTIC DATABASE (NED), references therein), make it the only quasar (and the must distant space object) that can be observed by amateur astronomers with small optical telescopes. Just like for the case of other AGNs, the conjecture is that at its core one can find a supermassive black hole. The mass of the SMBH at the centre of 3C 273 has been estimated to be between $M_{SMBH} \sim 10^8 M_\odot$ and $M_{SMBH} \sim 7 \times 10^9 M_\odot$ (Espaillat et al. (2008), Paltani and Türler (2005)), while the accretion-powered bolometric luminosity of 3C 273 was in previous studies estimated to around 10^{47} erg s^{-1} ((Paltani and Türler, 2005). The observed flux of the object was in the hard X-ray band (2-10 keV) estimated to be 7.87×10^{-11} erg cm^{-2} s^{-1} (Piconcelli et al., 2005).

It is commonly agreed that the source of energy in quasars, such as 3C 273, is the gravitational interaction between the SMBH and its accretion disk (Lynden-Bell, 1969), however the details of the very process are still far from understood. Even though it does exhibit some traditional spectral characteristics, previous studies have shown that 3C 273 is not a typical quasar - compared to others, it has a strong radio emission, including a significant continuum emission from the jet at lower radio frequencies (Henry et al., 1984).

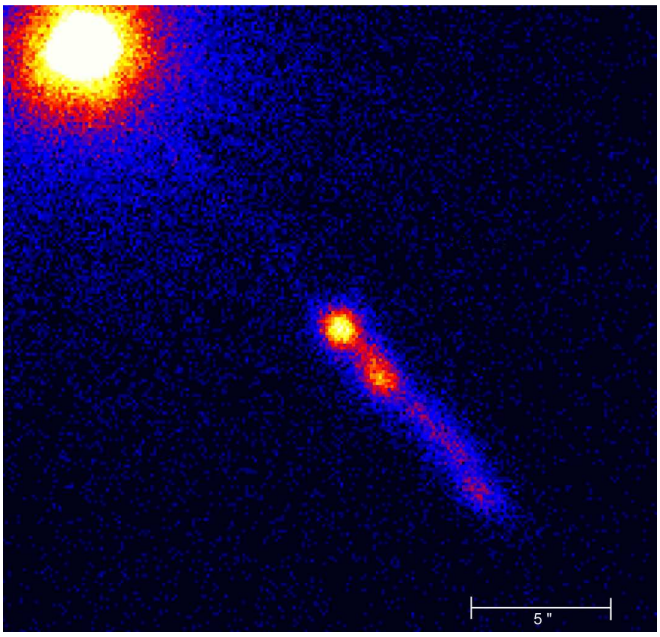

Figure 1.3: A picture of 3C 273 with its continuous jet from the centre, taken by *Chandra* X-Ray observatory. Such narrow jet of X-rays can stretch hundreds of thousands of light-years in length. Credit: NASA/CXC/SAO/H.Marshall et al.

Spectral energy distribution (SED) analysis shows that even though in some ranges power law is sufficient to describe the SED, over the whole SED it is not the most ideal (Perry et al., 1987). Using RGS data we are fitting the SED between 0.3 and 2 keV, so we will need both the power-law and the soft x-ray excess components.

Since its discovery and first characterisation in 1963, 3C 273 has been one of the most investigated AGNs in all spectral bands, but it has reached its peak in popularity thanks to X-ray absorption and emission line spectroscopy abilities of *Chandra* and *XMM-Newton* observatories (Soldi et al. (2008); Jester et al. (2006)). In the past, there has been quite some confusion and ambiguity about characterisation of 3C 273 as a blazar-type AGN, but as the latest *Chandra* pictures (see figure 1.3) and observations confirm, the jet is not pointing in our direction (Véron-Cetty and Véron, 2006). Moreover, its optical spectrum is characterised as Seyfert 1 type (Veron et al. 2006 catalogue).

X-ray spectroscopy of 3C 273 started with the identification of 3C 273 as an X-ray source by Bowyer et al. (1970) and Kellogg et al. (1971), with the detailed analysis of observations following from various rocket and satellite based X-ray instruments, such as *EINSTEIN* (Harris and Stern, 1987) and *ROSAT* observatory (Röser et al., 2000), and later by Sambruna et al. (2001) using the calibration data from *Chandra* observatory. In this thesis we will use the observational data from *XMM-Newton* Reflection Grating spectrometer (RGS) (den Herder et al., 2001) observatory (see sections 1.5, 1.6).

1.4 Power of high resolution X-ray spectroscopy

Before the advent of high-resolution X-ray spectrometers such as *Chandra* and *XMM-Newton*, low-resolution and blurred edges were the only way to investigate X-ray absorption by ionised outflows. Thanks to their high-spatial resolution (*Chandra*) and unprecedented high-throughput sensitivity (*XMM-Newton*), we can now detect X-ray absorption lines, which enable us to study ionised outflows even with weak absorption. Before the launch of *Chandra* and *XMM-Newton* observatories, only the continuum could be observed, such as the black body or power-law, as well as some broad edges. Now, the obtained spectra can be studied into much greater detail, and can be further analysed with more precise models. These satellites present a major breakthrough in space investigations - their high-spectral resolution do not only enable us to detect specific spectral lines of the elements, but can consequently also provide us with useful information about the structure and velocities of gases, while their higher effective areas enable us to detect much fainter objects, much further away. Higher spectral resolution and high sensitivity observations require spectral codes with high accuracy and reliability, in order to fit the complex spectra of AGN, and model the absorption and emission lines of astrophysical plasma. The software package called `SPEX`[2], which we will use for modelling in this thesis, has since 1992 been developed at the Space Research Organisation of The Netherlands (SRON) (Kaastra et al., 1996) (see section 2.1).

[2]http://www.sron.nl/spex

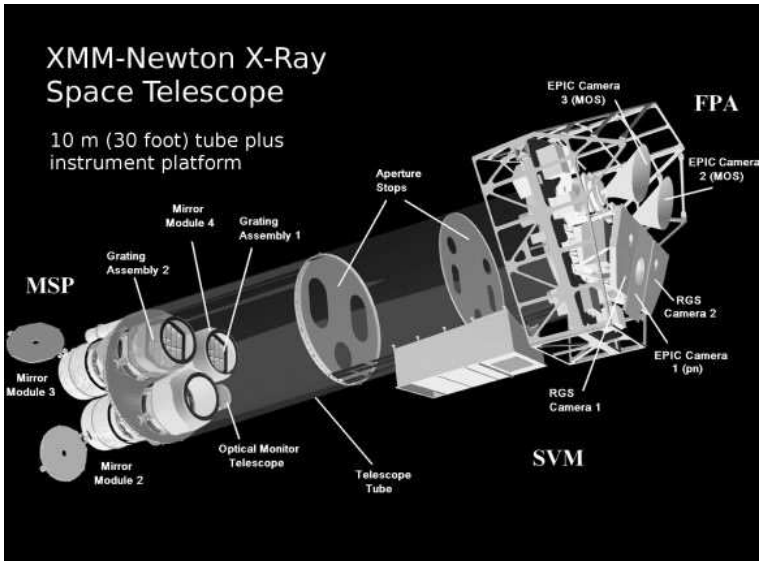

Figure 1.4: A scheme of the *XMM-Newton* observatory with its parts tagged. On the Focal Plane Assembly (FPA, right) are located the cameras - two Reflection Grating Spectrometers (RGS), an EPIC PN and two EPIC MOS imaging detectors. Credit: ESA/XMM-Newton

1.5 XMM Newton

In December 1999, European Space Agency (ESA) launched the most sensitive X-ray observatory ever put in space, X-ray Multi-Mirror Mission (*XMM-Newton*) (Jansen et al., 2001), named after physicist and astronomer Sir Isaac Newton. The spacecraft equipped with three high definition X-ray telescopes with high collecting area, is providing highly sensitive and precise narrow- and broad- range spectroscopy of interstellar X-ray sources (see figure 1.4). Since Earth's atmosphere blocks out all the X-rays, in order to perform meaningful and precise measurements we have to go beyond the atmosphere, which is what was one of the main motivational factors behind launching *XMM-Newton* (and *Chandra*). The detectors mounted on the satellite are two Reflection Grating Spectrometers (RGS) (den Herder et al., 2001), an European Photon Imaging Camera (EPIC) PN (Strüder et al., 2001) and two EPIC MOS imaging detectors (Turner et al., 2001). Using its high-quality sensors, *XMM-Newton* can investigate spectra of cosmic X-ray sources with the upper limit of flux of 10^{-15} erg cm^{-2} s^{-1}, and perform medium-resolution spectroscopy over the wavelength band between 5 and 35 Å (350 - 2500 eV), broad band imaging spectroscopy between 1 - 62 Å (0.2 - 12 keV), and using its optical monitor, a simultaneous sensitive coverage between 1700 and 6500 Å.

1.6 RGS - Reflection grating spectrometer

The cameras used in the analysis presented in this thesis are the two Reflection Grating Spectrometers (RGS 1, RGS 2) (den Herder et al., 2001), mounted behind two of the three Wolter I type mirrors nested on the XMM-Newton. They utilise about 53% of all the passing X-ray light. Each of the two RGS consist of an arrangement of reflection gratings that diffract the X-ray light into charge coupled devices (CCD) detectors (see figure 1.5). The instrument enables high resolution measurements ($E/\Delta E = 100$ to 500) in the soft X-ray band between 5 and 38 Å, (between 0.35 and 2.5 keV), with its maximum effective area of 150 cm^2 at 15 Å. The RGS was developed and constructed at Space Research Organisation of The Netherlands (SRON).

1.7 Motivation behind this study

As already mentioned in the previous sections, there are major uncertainties around the processes and factors influencing the production and launching of AGN winds, as well as the hot gas in the Milky Way. By conducting this study, we wish to further investigate, and check the validity of the previously known models for the structure of AGNs and the properties of the hot gas in the Galaxy. Determining the origin and the physical structure of the outflows as well as the warm absorbing Galactic gas, and understanding their role in shaping the spectra and variability are crucial for a good general understanding of the AGN and galaxy evolution. Being available for 'only' the last two decades, *Chandra* and *XMM-Newton* observatories are writing a new chapter of space explorations. Using their data we can learn a lot about not only distant and powerful objects, such as AGNs, but also about our very own place in the Universe.

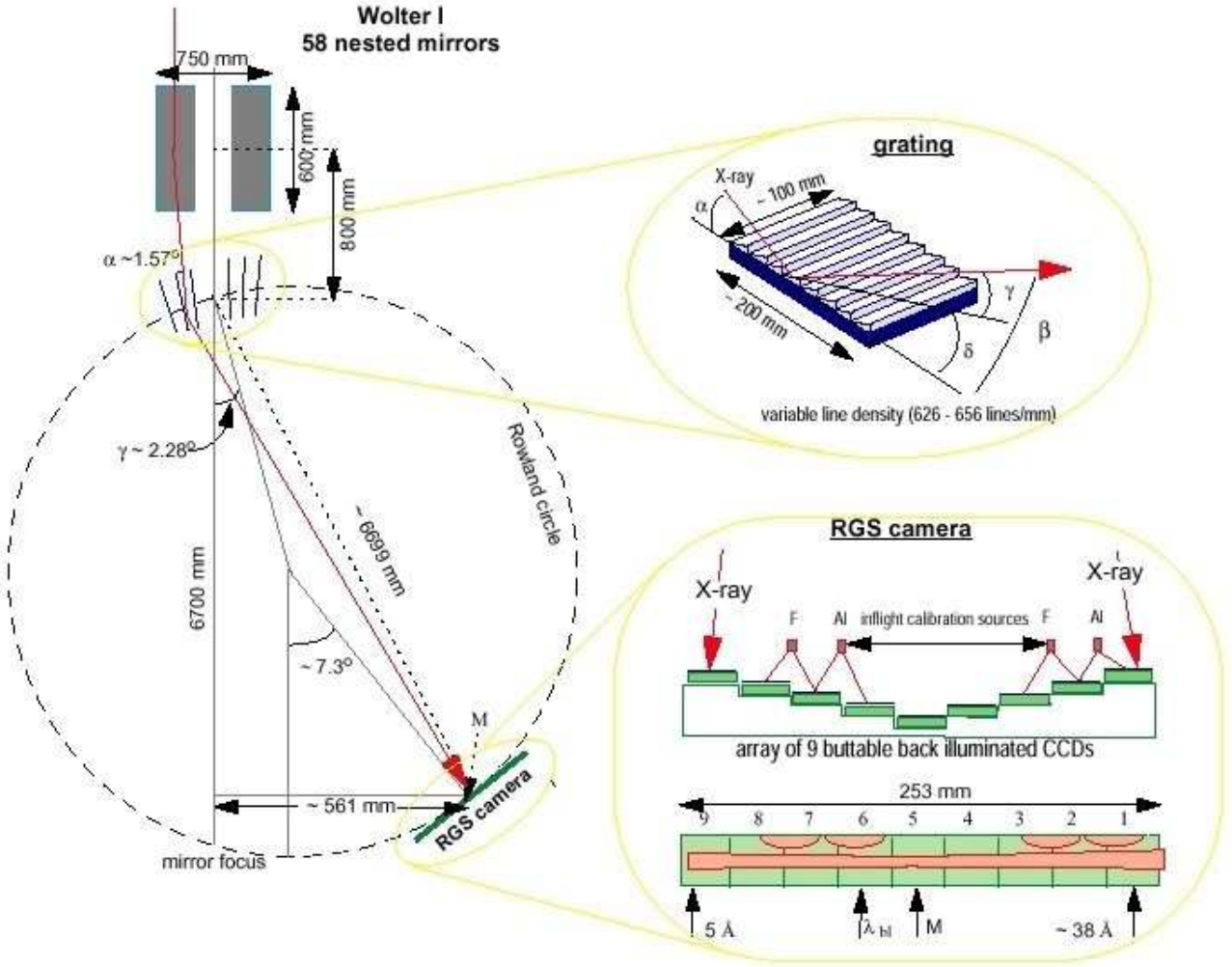

Figure 1.5: A scheme of the RGS sensor with its parts tagged. RGS composes of reflection grating array (RGA) that diffract the X-ray light into CCD detectors. Indicated are the numerical values for a few key dimensions and angles. Credit: Brinkman et al. (1998)

Chapter 2

Spectral modelling in SPEX

2.1 Data reduction

The data that will be analysed in the following chapters of this thesis were retrieved from the XMM-Newton Science Archive (XSA). Some of the numerical information about the data can be found in the left half of the Table 2.1. For the data reduction we follow the same procedure as described in Appendix A of the (Mehdipour et al., 2015b) paper, where the reduction of *XMM Newton* data of NGC 5548 is described. However, here for the stacking of the RGS spectra we use the `rgscombine` task of XMM Newton science analysis system (SAS). From a total of 42 observations a single stacked RGS spectrum was produced for spectral fitting. The data were taken with the Spectro+Q mode of the RGS instruments.

As already mentioned in the previous section, we will be modelling data using a `SPEX` package (Kaastra et al., 1996) version 3.04.00. `SPEX` is a spectral fitting command-line based program designed specifically to fit high-resolution X-ray spectra of hot plasma. The code includes several detailed models, which are able to describe and sufficiently plot radiative processes in the X-ray band. In the calculations `SPEX` uses some predefined cosmological parameters for luminosity computations, which are presented in Table 2.1, together with information about the stacked RGS spectrum of 3C 273.

Using the reduced data, we can plot the observed spectrum, and apply a model to it, one component a time. Namely, we would like to model the continuum, and the absorption and emission lines on the spectrum. After importing the data in `SPEX`, we start by changing the units and ranges of the axis, making them linear, and ignoring the parts where the sensitivity and calibration of RGS is not reliable anymore (below 6 and above 38 Å). We then bin the non-ignored data and define the cosmological distance of our object in terms of red-shift z of our object of investigation. Now we can start investigating *what* the data is showing. To explore that, our plan is as follows; firstly, we define general models that fit the continuum shape; secondly, using Gaussian function model we identify the emission and absorption lines, and find the wavelengths at which they occur; thirdly, from the list of known absorption and emission lines we identify the ions producing these lines based on their oscillator strength, and determine whether it is more likely that the absorption (or

Basic information about the data		Cosmological parameters in SPEX	
Data energy range (keV)	$0.31701 - 3.0996$	H_0 (km s^{-1} Mpc^{-1})	70
Net source counts	3810600 ± 2090	Ω_m	0.300
Net source count rate (counts/s)	1.9646 ± 0.0016	Ω_Λ	0.700
Mean exposure time (s)	2.08826×10^6	Ω_r	0
Number of data channels	3511		
Average integration time per channel (s)	2.08826×10^6		

Table 2.1: Basic statistical information about the data (left), and basic cosmological parameters as defined and adopted in SPEX for luminosity computation in our modelling (right).

emission) occurred in the Milky Way, or in the AGN; and lastly, we will attempt to model the AGN winds with the appropriate SPEX model. Throughout the modelling, we will be following the goodness of the fit of our model. This will be measured using C-statistics, and after applying new models, or changing the parameters, we will compare the new C-stat value with the old one, to show if, and how much, the model has been improved (see table 2.7 at the end of this chapter, for an overview of the overall improvement of the C-stat).

There is a couple of parameters that will not change throughout the modelling. First, as already described, in all of our modelling we will use the same cosmological red-shift value. Red-shift will not affect the lines produced within the Milky Way, however all lines associated with AGN 3C 273 do need to be red-shifted. We do this by defining a multiplicative model `reds`, which applies a red-shift z to a spectral component. For example, for a photon emitted at energy E.

The second fixed parameter applies only to the Milky Way, namely the neutral Milky Way absorption. When modelling the absorption in the Milky Way, we will use `hot` model in SPEX. `Hot` model calculates the transmission of gas in a collisional ionisation equilibrium. Given a temperature and a set of abundances, the model determines the ionisation balance, and then calculates all ionic column densities based on the prescribed total hydrogen column density. A lot of research has been done on the neutral absorbing gas in the Milky Way, so we can use previously calculated values for the total Galactic H I column density in the line of sight towards the 3C 273, $N_H = 1.79 \times 10^{20}$ cm^{-2} (Willingale et al., 2013). Using this, all ionic column densities can be determined, from which, by multiplying by the transmission of the individual ions, the total transmission of the plasma can be calculated. To produce the transmission of a neutral plasma in collisional ionisation equilibrium (such as the Galactic ISM), the temperature is set to 0.5 eV, which is the minimum allowed temperature for the model. (See Table 2.4)

2.2 Continuum

We start by modelling the biggest and the most obvious part of the spectrum: i.e. the power-law continuum. It has been shown that in the 2 - 10 keV region (and extending up to 1 MeV), 3C 273 can be well-represented by a power law (e.g. Grandi et al. (1997)). This power-law continuum follows from a non-thermal emission arising as a consequence of the inverse Compton up-scattering of disk photons in a hot ($T_e \sim 100$ keV), optically thin ($\tau \sim 1$) corona (e.g. Sunyaev and Titarchuk (1980); Haardt and Maraschi (1993)). The photon flux F as a function of a photon energy E can then be expressed with the power-law equation in the form

$$F(E) = AE^{-\Gamma}. \tag{2.1}$$

where we are fitting the normalisation constant, A, in units of 10^{44} ph s^{-1} keV^{-1} at 1 keV, and the photon index Γ of the spectrum. Using `pow` model in `SPEX`, we can fit the power-law model to our spectrum. The best-fit parameters of the `pow` model are presented in Table 2.2.

After fitting the power-law, we notice that the continuum cannot be fully fitted with solely the `pow` model - namely, at lower energies the spectrum is slightly steepened above an extrapolation of the power-law (see Figures 2.1 and 2.2). This feature is called the *soft X-ray excess*, and since its discovery in 1985 has been observed in the spectra of many AGN. This leads us to define another component of the continuum, which modifies blackbody radiation by coherent Compton scattering, `mbb` model (Rybicki and Lightman (1979), Kaastra and Barr (1989)). The very nature of this soft X-ray excess is still an active area of research, and many different explanations have been put forward. Currently the main four interpretations for the origin of the soft X-ray excess are (1) the high energy tail of the accretion disk's thermal emission (e.g. Arnaud et al. (1985)), (2) blurred relativistic photoionised reflection from the disk, as modelled by Ross and Fabian (2005) (e.g. Crummy et al. (2006)), (3) remains of smeared ionised absorption in a relativistic wind from the inner disk (e.g. Gierliński and Done (2004)), and (4) 'warm' Comptonisation, where the process is very similar to the one producing the power-law shape, but relating to the corona of lower temperature and of higher optical depth (e.g. Magdziarz et al. (1998); Done et al. (2012); Middleton et al. (2009)). The latter is probably the most widely accepted one, and also an explanation we will make use of in this thesis, using `mbb` model. A comparison of the plots and C-statistics, with and without this `mbb` modification can be seen in figures 2.1 and 2.2.

The measurements of fluxes and luminosities of continuum of 3C 273 through `SPEX` reveal the value of the energy flux to be 5.437 $\times 10^{-11}$ erg cm^{-2} s^{-1} and the bolometric luminosity to be 4.017 $\times 10^{45}$ erg s^{-1} in the hard X-ray band (2 - 10 keV), which are slightly lower than, but close to the values offered by Piconcelli et al. (2005) and Paltani and Türler (2005) (and presented in section 1.3). The values for the energy flux and luminosity for the soft X-ray bound (0.2 - 2 keV) are 7.302 $\times 10^{-11}$ erg cm^{-2} s^{-1} and 6.583 $\times 10^{45}$ erg s^{-1}, respectively.

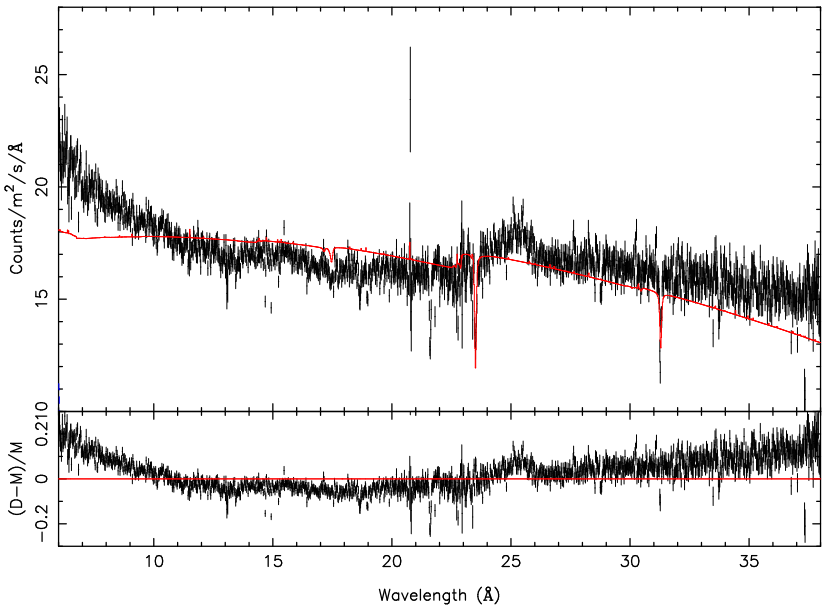

Figure 2.1: A figure of the fitted model (red line), when the continuum is fitted only with the power-law (`pow`) model (+ neutral `hot` model). The C-statistics for this fit is 8193.56/1612.14.

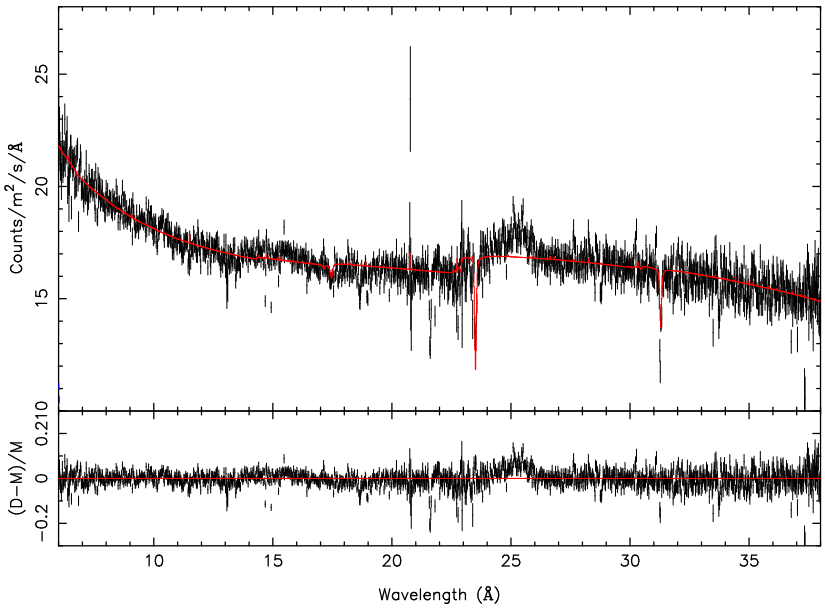

Figure 2.2: A figure of the fitted model (red line), when the continuum is fitted both with the power-law (`pow`) and the modified black body `mbb` model (+ neutral `hot` model). The C-statistics for this fit is 6084.01/1612.14.

Table 2.2: Best-fit parameters of the continuum model of our spectrum.

Parameter	Value
Primary power-law component (`pow`):	
Normalisation (1E54 ph/s/keV)	1.056 ± 1
Photon index Γ	2.54 ± 0.01
Modified black body (`mbb`):	
Normalisation (1E32 $m^{0.5}$)	3.88 ± 0.2
Temperature (keV)	1.795 ± 0.05

2.3 Absorption line identification

With a continuum model set, we can now focus on smaller features of the spectrum. Namely, we are interested in investigating the absorption (and emission) lines. By applying the `gaus` component in `SPEX`, we fit the peaks and troughs along the spectrum, and identify at which wavelength they are appearing in the spectrum. The `gaus` function is given by

$$F(E) = Ae^{(E-E_0)^2/2\sigma^2} \tag{2.2}$$

where F is the photon flux (in units of 10^{44} ph s^{-1} keV-1), E is the photon energy (in keV), A is the line normalisation factor (units of 10^{44} ph s^{-1}), and E_0 is the central energy of the spectral line (in keV). `SPEX` provides us with an option of defining the wavelength (in the units of Å) instead of energy (in keV), to make the use for dispersive spectrometers easier. Finally, σ represents the Gaussian width, which we can relate to the full width at half maximum (FWHM) by $FWHM = \sigma\sqrt{\ln 256}$. Using this method we identify several of the strongest lines, and note down their wavelengths, normalization factors and FWHMs (results given in table 2.3). An important thing to keep in mind is that if the absorption happened at 3C 273, then the line as detected by *XMM-Newton* will be red-shifted. As we already know the red-shift of 3C 273 we can calculate the intrinsic wavelength at which the absorption happened, using

$$\lambda_{0,3c273} = \frac{\lambda_{observed}}{1+z}, \tag{2.3}$$

where $z = 0.158339[0.000067]$, (Strauss et al., 1992). Using the `SPEX` list of line wavelengths and their oscillator strengths for different ions, we can determine whether the absorption line belongs to the AGN or the Milky Way. The strongest absorption lines in the RGS spectrum are identified in Table 2.3 and labelled in Fig. 2.3.

Table 2.3: The table of the biggest identified absorption lines, together with the identification whether the absorption occurred at 3C 273 (and the line is red shifted) or in the Milky Way. λ_0 for the 3C 273 was calculated using Eq. 2.3. The values of the theoretical wavelengths and the oscillator strengths are from the atomic database of SPEX 3 (see the SPEX manual for more details).

$\lambda_{obs} = \lambda_0$ (if Galactic) (Å)	Gaus Normalisation (1E37 ph/s)	FWHM (Å)	λ_0 (if 3C 273) (Å)	Galactic or 3C 273	Ion ID	Intrinsic wavelength	Oscillator strength
$18.657^{+0.006}_{-0.007}$	-1.7 ± 0.2	0.07 ±0.03	$16.107^{+0.005}_{-0.006}$	Galactic	O VII	18.6288	1.46 $\times 10^{-1}$
$18.969^{+0.006}_{-0.005}$	-1.4 ± 0.1	0.03 ±0.03	$16.377^{+0.005}_{-0.004}$	Galactic	O VIII	18.9725	1.39 $\times 10^{-1}$
21.607 ± 0.003	-2.6 ± 0.2	$0.01^{+0.02}_{-0.01}$	18.654 ± 0.003	Galactic	O VII	21.6019	6.96 $\times 10^{-1}$
23.10 ± 0.01	-1.1 ± 0.2	$0.02^{+0.04}_{-0.02}$	19.943 ± 0.009	Galactic	O III	23.1092	1.26 $\times 10^{-1}$
23.330 ± 0.009	-9.5 ± 0.2	$0.0003^{+0.07}_{-0.0003}$	20.141 ± 0.008	Galactic	O II	23.3514	1.01 $\times 10^{-1}$
23.51 ± 0.03	-3.2 ± 0.2	0.04±0.01	$20.298^{+0.003}_{-0.03}$	Galactic	O I	23.5114	1.04 $\times 10^{-1}$
28.79 ± 0.01	-1.0 ± 0.2	¡ 0.03	24.851 ± 0.009	Galactic	N VI	28.787	6.75 $\times 10^{-1}$
$31.273^{+0.001}_{-0.008}$	-3.0 ± 0.2	$0.001^{+0.04}_{-0.001}$	$26.9991^{+0.0007}_{-0.007}$	Galactic	N I	31.2865	1.01 $\times 10^{-1}$
33.737 ± 0.009	-1.4 ± 0.2	$0.01^{+0.02}_{-0.01}$	29.126 ± 0.008	Galactic	C VI	33.7396	1.39 $\times 10^{-1}$

2.4 Hot Milky way absorption

In the previous section we identified all of the strongest lines to be Galactic, meaning that the absorption occurred in the Milky Way and is therefore not red-shifted. In the same manner, as we at the beginning of our modelling set the neutral `hot` model for the absorptions in the Milky Way, we now define two more `hot` models, which will fit the absorption lines occurring at higher temperatures, as it is clear that only one `hot` model does not provide a good fit for all the absorption lines. As we already know the total Galactic H I column density in the line of sight towards the 3C 273, we will simply start with this value and free the column density and the temperature parameters, in case `SPEX` finds a best-fit to the lines. At different temperatures, different absorption lines will be modelled self-consistently - not only the strongest that we identified in the table above, thus, the weaker absorption lines belonging to gas with a given temperature are also modelled. In `SPEX`, using `asc ter transmission` and `asc ter column` commands, we can check which absorption lines, and how deep, will occur in gas of different temperatures in a collisional ionisation equilibrium. Through experimenting we determine three `hot` models (cold; ~ 0.0005 keV, warm; ~ 0.01 keV, hot; ~ 0.1 keV), which sufficiently fit the majority of the identified lines. Lastly, we free the velocities of the `hot` models, and let `SPEX` fit it in the best way. The results, and the values of parameters with errors of all three models can be found in table 2.4. For the improvement of the C-stat after applying each model, see table 2.7.

Table 2.4: Best-fit parameters of our model for the Milky Way absorption. The velocity parameter refers to the "shift" velocity, i.e. the velocity of the enitre slab of gas.

Parameter	Value
Milky Way X-ray Absorption Models (`hot`) (1/3):	
X-Column (1E23/m^2)	17.7 (f)
Temperature (eV)	0.5 (f)
Average velocity (km/s)	-2^{+10}_{-90}
Milky Way X-ray Absorption Models (`hot`) (2/3):	
X-Column (1E23/m^2)	$6.26^{+0.4}_{-0.5}$
Temperature (eV)	133 ± 3
Average velocity (km/s)	102^{+21}_{-44}
Milky Way X-ray Absorption Models (`hot`) (3/3):	
X-Column (1E23/m^2)	1.93 ± 0.4
Temperature (eV)	9.59 ± 0.6
Average velocity (km/s)	450^{+114}_{-84}

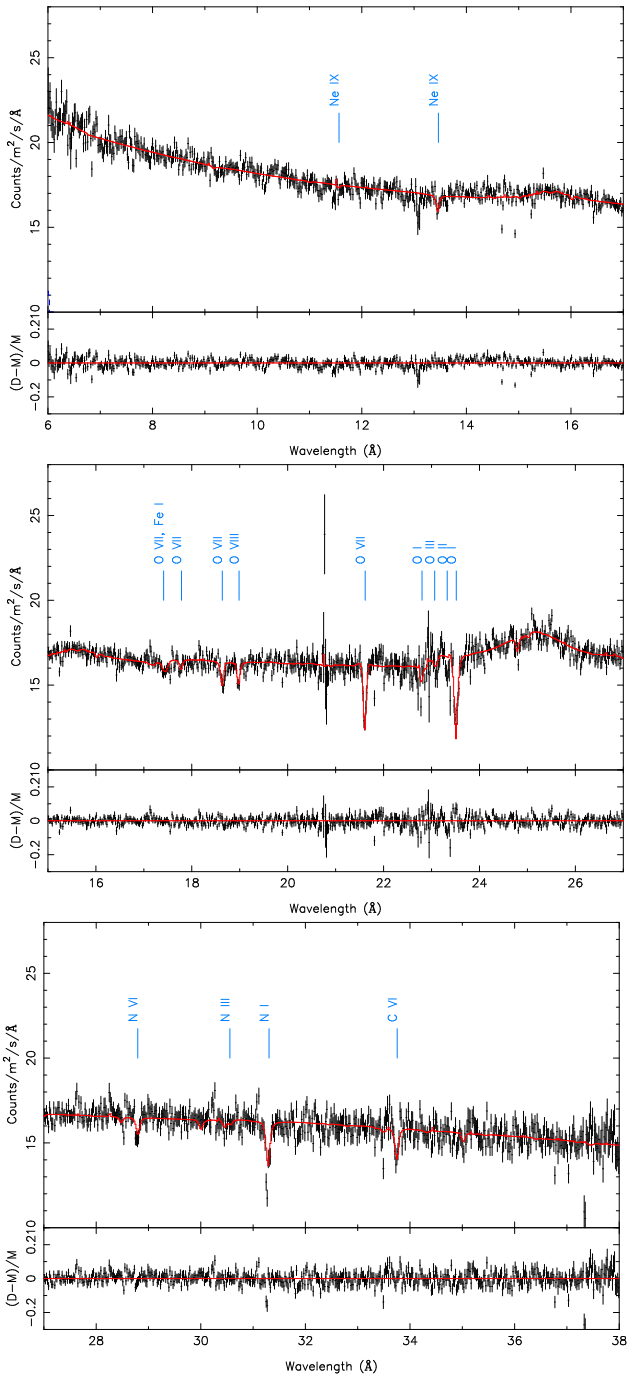

Figure 2.3: Different parts of the RGS spectrum (6 - 17 Å; 15 - 27 Å; 25 - 38 Å) with the strongest identified lines labelled. The model was fitted after applying three `hot` models, each at a different temperature. The first absorption line in the second part (15 - 27 Å), indicated as O VII, Fe I is a superposition of the absorption lines of those two ions.

2.5 Broad emission lines

After fitting the absorption lines in the spectrum we are still left with some residuals, so we also want to fit those emission lines. In hotter gasses, the strongest emission lines will be produced by hydrogen and helium like ions, so we are expected to see those first in the spectrum, meaning that we would be expected to see the O VII and O VIII lines first. We find that the wavelengths of the residuals in the RGS spectrum are consistent with the wavelengths of known He-like triplet emission lines, so we will proceed by fitting delta lines at the corresponding wavelengths, and then broaden them sufficiently. `SPEX` allows modelling the lines using `delt` model, and applying the Gaussian broadening model to them using `vgau` model. He-like triplets originate from cooling of hot gas containing He-like ions (such as C V, N VI, O VII, Ne IX). They correspond to three different transitions of a He-like element: the w resonance line (transition form $1s^2\ ^1S_0$ to $1s\ 2p\ ^1P_1$), the x and y intercombination lines (transition from $1s^2\ ^1S_0$ to $1s\ 2p\ ^3P_{2,1}$, respectively) and the z forbidden line (transition from $1s^2\ ^1S_0$ to $1s\ 2s\ ^3S_1$) (see figure 2.4). The relative intensities of the triplet transition lines is often used for temperature and density diagnostics and the analysis of the coronal collisional and photoionised plasma (Gabriel and Jordan, 1969). Since the O VII and Ne IX triplets occur at around 21.6 Å (w) 21.8 Å (x, y), 22.1 Å (z), and 13.4 Å (w), 13.6 Å (x, y), 13.7 Å (z), respectively, which lie well within the band of our X-ray spectrum, even if red-shifted, we expect and indeed detect those lines. After fitting those two emission residuals belonging to O VII and Ne IX, we can see another

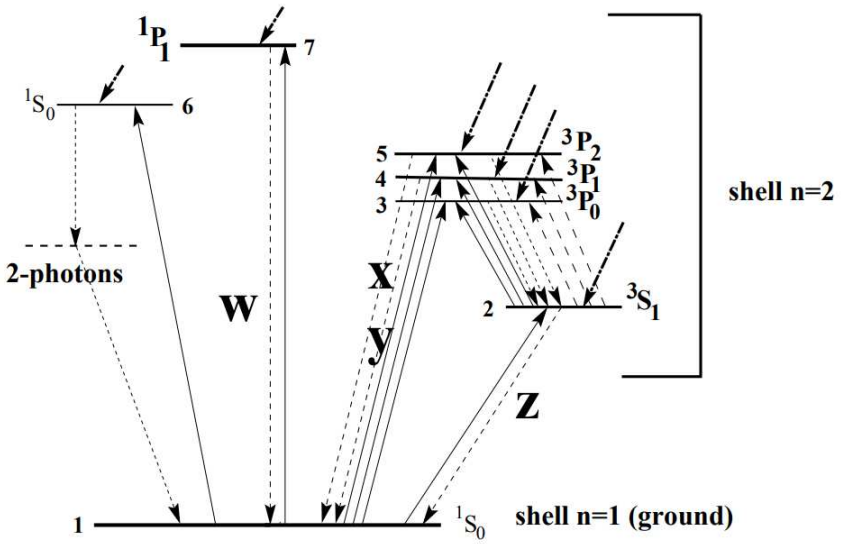

Figure 2.4: A Grotrian diagram of He-like transition between the energy levels showing the resonance (w), intercombination (x, y) and forbidden (z) transitions. Upward arrows represent excitation, i.e. absorption, and the downward arrows represent emission. Source: Porquet et al. (2001)

one, still undefined at around 22 Å. Since there is no He-like ion that produces lines in the vicinity of (or one whose red-shift would correspond to) that value, this emission line had to be produced by a H-like ion. Indeed, upon further investigation we notice that the set of lines responsible for that emission are the O VIII Lyman-α (Ly-α) doublets (which will be due to such small difference in their wavelengths modelled as one). Those lines appear when an electron falls from the $n = 2$ orbital to the $n = 1$ orbital, and its expected wavelength is around 19 Å (which when red-shifted fits the bump relatively well). As mentioned before, for the case of all three emissions (two triplets and a doublet) we do need to consider the red shift as well.

We model the triplets by representing them with delta lines in the spectrum at the theoretical wavelengths, by using `delt` model. `Delt` model is a simple model which generates an infinitely narrow emission line. Its spectrum is given by

$$F(E) = A\delta(E - E_0), \tag{2.4}$$

where F is the photon flux (in units of 10^{44} ph s^{-1} keV-1), E is the photon energy (in keV), A is the line normalisation (units of 10^{44} ph s^{-1}) and E_0 is the line energy of the spectral line (in keV). Similarly as in the case of `gaus` model, for easier use we can switch between the basic units given in terms of energy or wavelength. Secondly, we define another component, namely `vgau` - Gaussian velocity broadening model. This model provides a *Doppler line broadening* model, resulting from a distribution of velocities within a gas (some parts of the gas are moving towards us, while other away from us). For all of the triplets of the same ion, we will assume that those velocities are same, so only one `vgau` per ion. The model broadens an arbitrary component with a Gaussian Doppler profile, which is characterised by the Gaussian velocity broadening σ (in units of km/s). For all three cases, we will keep the velocity parameter freed, so `SPEX` fitting can adjust it to the best-fit velocity. However, there is another effect, produced by a different kind of velocity: the *Doppler shift* of the lines (not to be mistaken with the cosmological Doppler shift, resulting from the expansion of the Universe), which arises due to the *flow velocity*, i.e. the whole gas medium moving either towards us or away form us. The flow velocity, responsible for the Doppler shift of the lines, can be calculated using the observed and the theoretical wavelengths of the emission lines via

$$v = \frac{\lambda_{obs} - \lambda_0}{\lambda_0} \times c. \tag{2.5}$$

Since for the case of O VII and Ne IX we used the theoretical wavelengths, which fit the spectrum sufficiently well, we can assume that their flow velocities are ~ 0 as it is consistent with the residuals. For the case of Ly-α line, we can however calculate the flow velocity using the equation 2.5, which results to the drift velocity of 5.02×10^6 m/s. The relative broadening velocities are calculated by `SPEX` based on the best fit model for an emission line. The wavelengths and names of the observed emission lines, as well as their broadening velocities are given in table 2.5. For the improvement of our C-stat after plotting each set of emission lines see table 2.7. The emission lines present in the spectrum are identified in figures 2.5 and 2.6

λ_{obs} (Å)	Norm Value (1E51 ph/s)	λ_0 (Å)	Transition ID	Broadening velocity (km/s)	δC-stat
13.44710 (f)	$1^{+0.8}_{-0.6}$		Ne IX - resonance transition		
13.55140 (f)	$0.7^{+1}_{-0.7}$		Ne IX - intercombination transition	7100^{+1300}_{-840}	-157.21
13.69870 (f)	$2^{+6}_{-0.8}$		Ne IX - forbidden transition		
18.649 ± 2e-2	$1.4^{+0.4}_{-0.3}$	18.9671	O VIII - Ly-α line	990^{+520}_{-370}	-18.56
21.60200 (f)	5 ± 2		O VII - resonance transition		
21.80700 (f)	6 ± 1		O VII - intercombination transition	5678^{+370}_{-350}	-456.69
22.10120 (f)	$0.3^{+1}_{-0.3}$		O VII - forbidden transition		

Table 2.5: By using `delt` line plotting we identified emission lines, namely triplets and a Ly-α doublet. The theoretical wavelengths are from the atomic database of SPEX 3 (see the SPEX manual for more details).

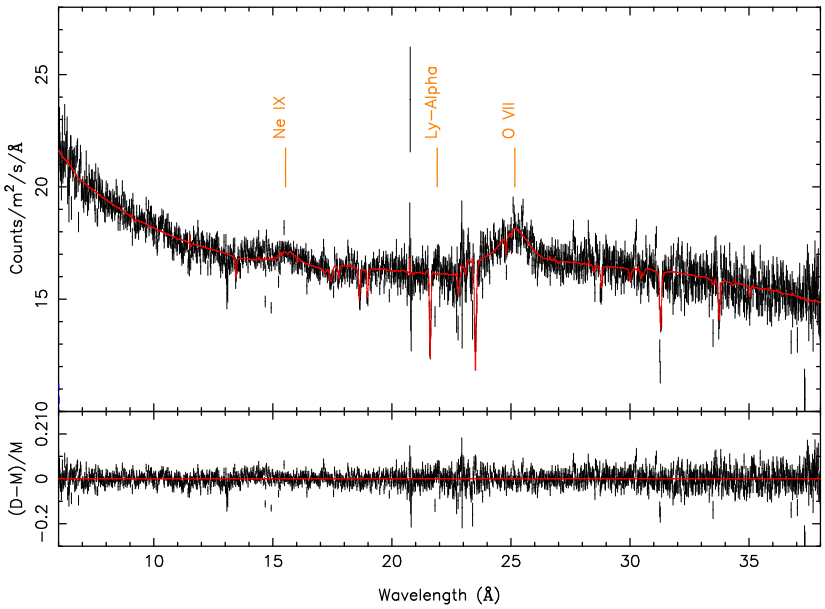

Figure 2.5: Final best-fit model (red line) over the whole observed spectrum (6 - 38 Å), when fitted with all the models as introduced in this chapter. Indicated are the locations of the emission lines as identified in the table 2.5.

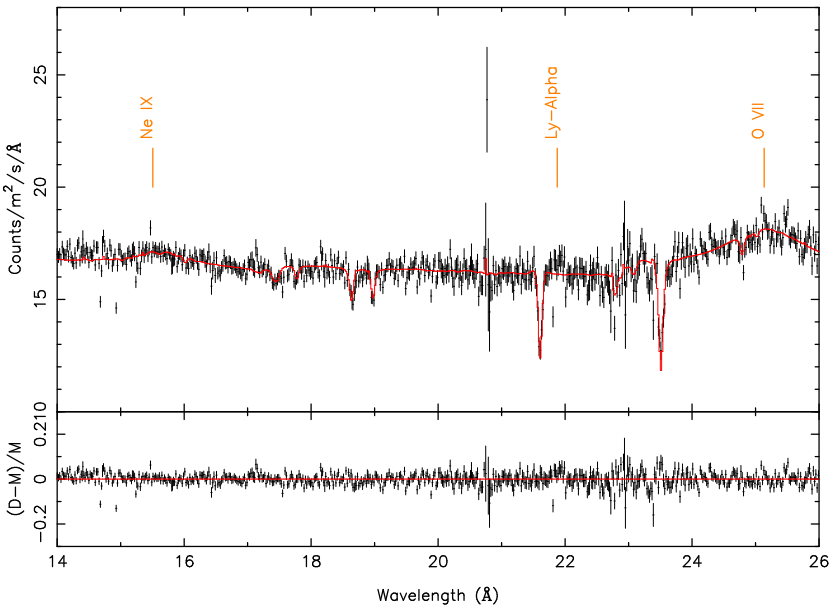

Figure 2.6: A close-up of the final best-fit model (red line), when fitted with all the models as introduced in this chapter. Indicated are the locations of the emission lines as identified in the table 2.5.

2.6 Searching for the AGN wind absorption lines

Lastly, with the aim of further improving the spectrum and identifying the smaller, weaker lines, we apply a physical model to fit the absorptions happening in a potential AGN wind. To do so, we define a new component in our model, called `xabs` model (Steenbrugge et al., 2005). The model calculates the transmission of a slab of material in which all the ionic column densities are connected through a photoionisation model. As opposed to the `hot` modelling of the collisional absorptions in the coronal plasma in the Milky Way, in the case of AGN the gas is ionised by radiation, thus this is a photoionised plasma. The model will mostly depend on the ionisation parameter $\xi = L/nr^2$, where L is the luminosity of the source, N the column density, and r the distance from the source. Other parameters are the hydrogen column density (in $10^{28}m^{-2}$), root mean square (RMS) velocity of the slab of material, and the velocity shift of the medium. Best-fitted parameters for those variables are presented in Table 2.6, and the C-stat improvement resulting from the `xabs` model is presented in Table 2.7. This was the last component added to our model..

Table 2.6: Best-fit parameters of our `xabs` model for fitting possible absorption from the AGN wind.

Parameter	Value
AGN winds model (`xabs`):	
NH (1E22/m^2)	1.9^{+2}_{-1}
Log xi (1E-9 Wm)	$1.275^{+0.4}_{-0.3}$
RMS Velocity (km/s)	110^{+580}_{-110}
Average velocity (km/s)	-38^{+410}_{-14000}

2.7 C-statistics improvement

Improvement	C-stat	δ C-stat
Continuum models:		
Power-law model (`pow`)	8193.56	-
Modified black body model (`mbb`)	6084.01	2109.55
Absorption models:		
First hot model (T $\sim$ 5e-4 keV) (`hot`)	3687.50	2396.51
Second hot model (T $\sim$ 1e-1 keV) (`hot`)	3309.04	378.46
Third hot model (T $\sim$ 1e-2 keV) (`hot`)	3166.27	142.77
Emission triplet lines:		
O VII triplets (`delt`)	2709.58	456.69
Ne IX triplets (`delt`)	2552.37	157.21
O VIII Ly-α line (`delt`)	2533.81	18.56
AGN winds		
AGN winds model (`xabs`)	2526.10	7.71
Velocity modifications		
Fixing the velocity of `hot` models	2498.50	27.6

Table 2.7: The improvement of C-statistics through attaching different models. The table is in chronological order - each new line in the table represents a new model added to all the previous ones. The expected C-stat is 1612.14 $\pm$ 56.79.

The final C-stat for the best fit model to the spectrum (as seen in figures 2.7 - 2.9) that we obtained during the fitting is

$$2498.50/1612.14 \pm 56.79. \tag{2.6}$$

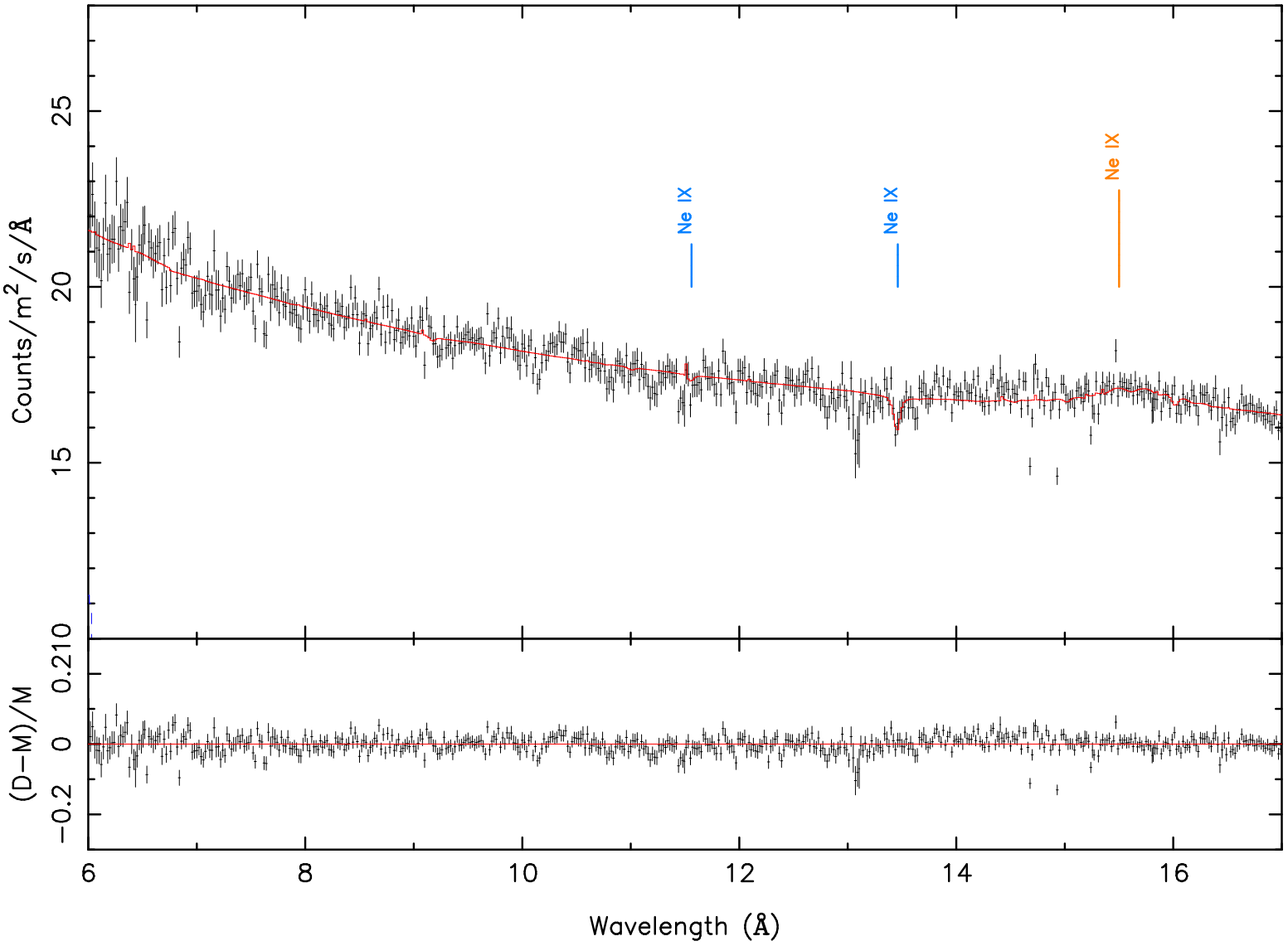

Figure 2.7: Final best-fit model, including the plot of residuals in the range 6 - 17 Å with all components as introduced in this chapter, with indicated absorption (blue) and emission (orange) lines.

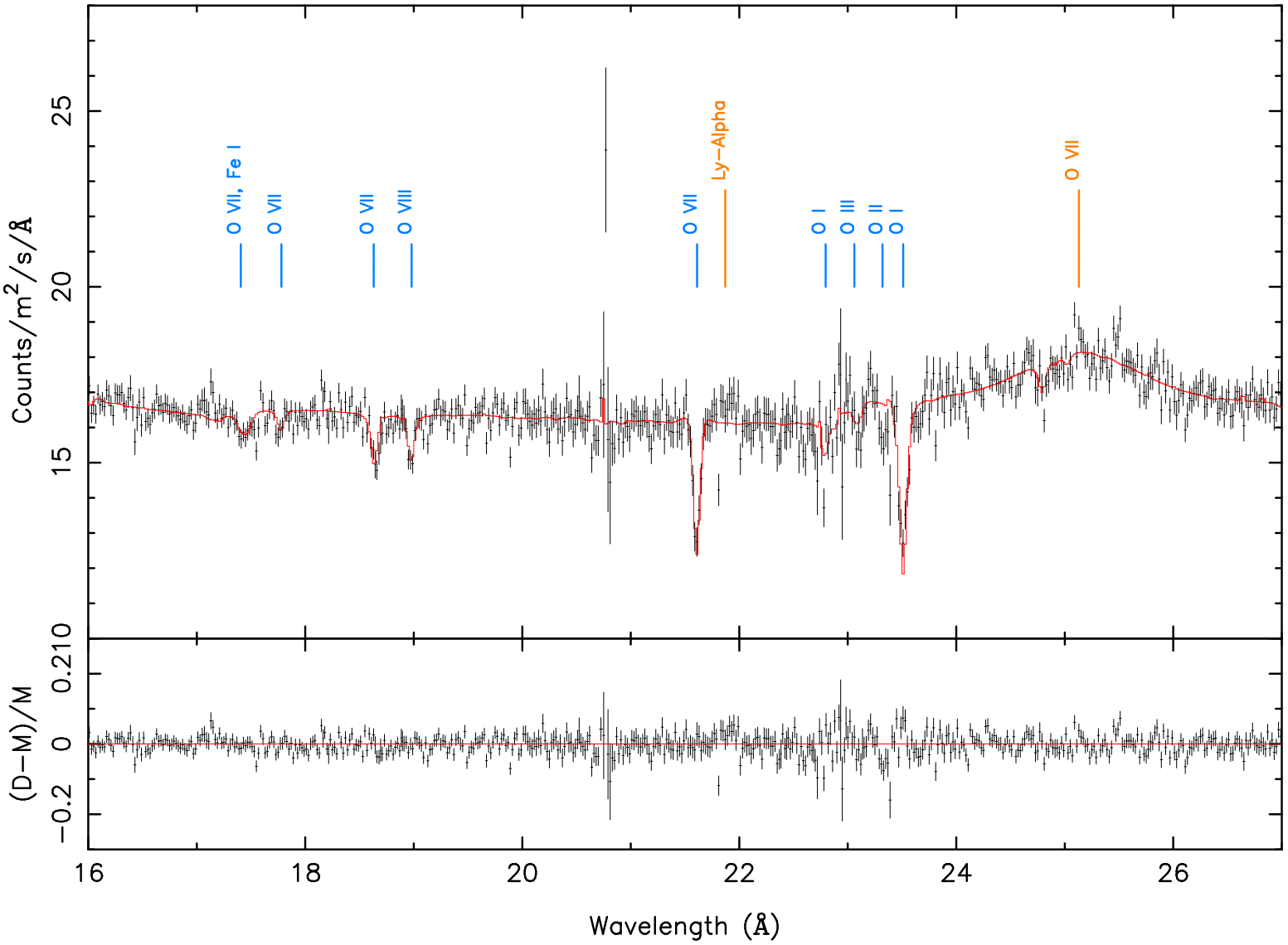

Figure 2.8: Final best-fit model, including the plot of residuals in the range 16 - 27 Å with all components as introduced in this chapter, with indicated absorption (blue) and emission (orange) lines.

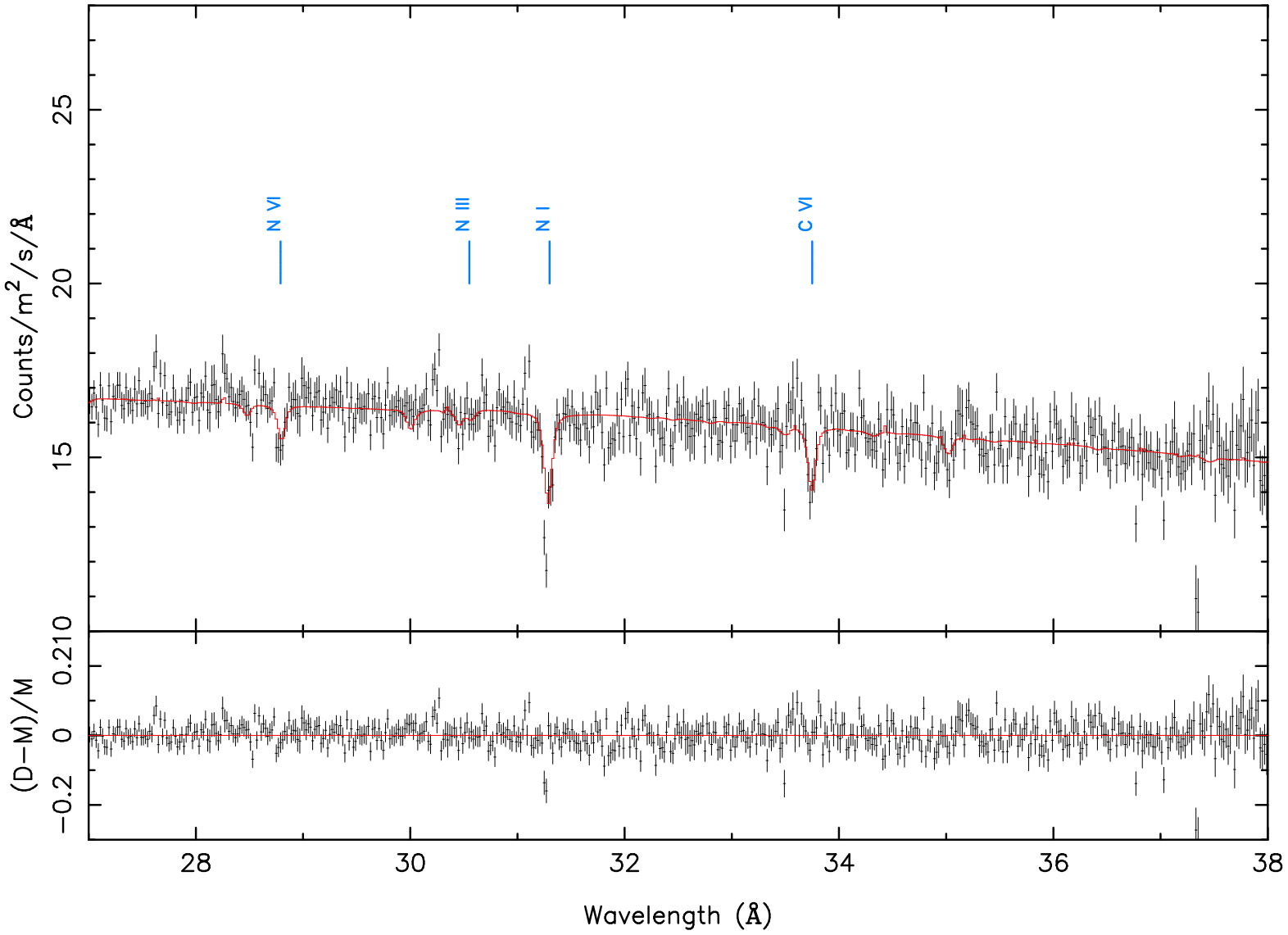

Figure 2.9: Final best-fit model, including the plot of residuals in the range 27 - 38 Å with all components as introduced in this chapter, with indicated absorption lines.

Chapter 3

Discussion

3.1 AGN structure

The region in the AGN responsible for the broad emission lines is simply known as broad line region (BLR). While a common consensus has been reached about a SMBH/accretion disk paradigm, the structure and the models describing broad emission lines are still poorly understood. The BLRs are located in the vicinity of the central engine, so it seems likely that the accretion disk and outflows play an important role in the structure and properties of those regions, which is where we will start our discussion. From the analysis done in section 2.5 we conclude that the BLR in 3C 273 consists of 3 components, with different broadening velocities. For the case of Ne IX and O VII no addition drift velocity was needed, since solely the cosmological red-shift shifted the theoretical wavelengths to the ones observed in the spectrum. However, for the case of Ly-α line the drift velocity was calculated to be around 5000 km/s. BLRs have been extensively observed and studied throughout the missions carried out by International Ultraviolet Explorer (IUE) satellite (Boggess et al., 1978), which is in particular very well adapted to the wavelengths around the Ly-α emission, of sufficiently red-shifted object, such as 3C 273. The velocities calculated and presented in this thesis are in an agreement with numerous observations conducted by satellites such as IUE, which estimate the upper limit of the drift velocity of Ly-α emitting gas in 3C 273 to be around 10000 km s^{-1} (e.g. Paltani and Türler (2003)).

As last, we made use of `xabs` model to determine the photoionised plasma absorptions occurring in the AGN wind. `SPEX` fit lines consistently, meaning that if it detects one of the potential lines, it will only fit it, if the other associated lines are also present in the spectrum. However, the best-fit model can only set an upper limit as the presence of these lines is not significant as N_H is relatively low, and therefore does not substantially improve the fit to the spectrum ($\delta C - stat = 7.71$). This suggests that in some radio-loud AGN, the wind may not be present. Nevertheless, many further statistical and data analyses will be needed in order to fully conclude and determine the relation between the AGN jets, and its winds.

3.2 Hot gas in the Milky Way

Through observational data we have shown that in order to sufficiently fit the vast majority of the absorption lines, we have to include three different phases of the Galactic ISM, hereafter usefully named the 'cold', 'warm', and 'hot' component. The cold, or the neutral component, set to the lowest temperature of $kT \sim 0.5$ eV (~ 5800 K) provided with of the neutral and low-ionisation lines, such as O I, N I, and Fe I. The warm component, $kT \sim 10$ eV (1×10^5 K), consists of mostly mildly ionised gas in a photoionisation equilibrium, and it gives rise to O II and O III. The third and the hottest of the `hot` models, $kT \sim 130$ eV (1.5×10^6 K), fits the highly ionised gas, and models the majority of the visible absorption lines, C VI, N VI and O VII. The detection of those absorption lines confirms previous observations of the Galactic hot gas in that general direction (e.g. Fang et al. (2002), Fang et al. (2003), Mathur et al. (2003)), while many papers also identifies the O VI absorption line at much higher wavelength (e.g. Sembach (2001)), which is a sign of high (positive) velocity clouds (HVC) in that line of sight. The problem is, that none of the corresponding absorption lines occur, and the most likely conclusion is that the O VI absorption line traces its origin from the Galactic fountain. In our case, the O VI was plotted by the second applied `hot` model, at ~ 130 eV, and the shift velocity of $\sim 102^{+21}_{-44}$ km/s. This value is relatively well matched with the shift velocity of gas responsible for the O VI absorption detected in the UV range (at 1032.35 Å), in the study done by Collins et al. (2005). They estimated the velocity to be in the range $105 < v < 240$ km/s, in order to establish 3σ upper limits on column densities involving other ion species. For the analysis of the Galactic ISM, we used a column density as given by Willingale et al. (2013), and used it as a fixed value of the first hot model. For the other two, we estimated it close to that range, an best-fit models show that also the other two hot models fit the graph best when the hydrogen column density is roughly of the same magnitude, within the factor of 10.

Chapter 4

Conclusion

In this paper we carried out the high resolution spectroscopy of 3c273, using data collected by *XMM-Newton* Reflection Grating Spectrometer. From the results of spectroscopy we conclude the following:

- The majority of the absorption occurred in three different phases of Milky Way, each part with its characteristic temperature - ~ 0.5 eV, ~ 10 eV and ~ 130 eV, and it's characteristic velocity - ~ -2 km/s, $/sim450$ km/s and ~ 100 km/s, respectively.
- The emission within the 6 - 38 Å X-ray band can very well be modelled using a power-law and a modified black body models, which lead us to believe that the the continuum shape of the emission-absorption graph arises as a consequence of Compton (up-)scattering of photons in a hot and optically thin corona (power-law), and in corona of lower temperature and higher optical depth.
- Beside the main continuum emission, we notice the occurrence of the distinct emission lines from the BLR, in the form of triplets, and Ly-α emission line. The drift velocities of the BLR are for the case of O VII and Ne IX (close to) zero, while the drift velocity of the gas producing Ly-α line was calculated to be around 5 $\times 10^6$ km/s. Due to the velocity distribution of the ions, within the gas itself, the broadening velocity could be determined as well: 5000 - 8000 km/s for the case of O VII and Ne IX, and roughly 1000 km/s for the case of Ly-α doublet.
- Using `xabs` model to plot the absorption happening in the AGN wind does not significantly improve our fit, meaning that not a lot of wind is present in around 3C 273, which is in agreement with the observations of the majority of the radio-loud AGNs.

Bibliography

Arnaud, K. A., Branduardi-Raymont, G., Culhane, J. L., Fabian, A. C., Hazard, C., McGlynn, T. A., Shafer, R. A., Tennant, A. F., and Ward, M. J. (1985). EXOSAT observations of a strong soft X-ray excess in MKN 841. *MNRAS*, 217:105–113.

Blaauw, A., Gum, C. S., Pawsey, J. L., and Westerhout, G. (1960). The new I. A. U. system of galactic coordinates (1958 revision). *MNRAS*, 121:123.

Boggess, A., Carr, F. A., Evans, D. C., Fischel, D., Freeman, H. R., Fuechsel, C. F., Klinglesmith, D. A., Krueger, V. L., Longanecker, G. W., and Moore, J. V. (1978). The IUE spacecraft and instrumentation. *Nature*, 275:372–377.

Bowyer, C. S., Lampton, M., Mack, J., and de Mendonca, F. (1970). Detection of X-Ray Emission from 3c 273 and NGC 5128. *ApJ*, 161:L1.

Brinkman, A., Aarts, H., den Boggende, A., Bootsma, T., Dubbeldam, L., den Herder, J., Kaastra, J., de Korte, P., van Leeuwen, B., Mewe, R., Paerels, F., de Vries, C., Cottam, J., Decker, T., Kahn, S., Rasmussen, A., Spodek, J., Branduardi-Raymont, G., Guttridge, P., Thomsen, K., Zehnder, A., and Guedel, M. (1998). The Reflection Grating Spectrometer onboard XMM. In *Science with XMM*.

Collins, J. A., Shull, J. M., and Giroux, M. L. (2005). Highly ionized high-velocity clouds: Hot intergalactic medium or galactic halo? *The Astrophysical Journal*, 623(1):196.

Crenshaw, D. M., Kraemer, S. B., Boggess, A., Maran, S. P., Mushotzky, R. F., and Wu, C.-C. (1999). Intrinsic Absorption Lines in Seyfert 1 Galaxies. I. Ultraviolet Spectra from the Hubble Space Telescope. *ApJ*, 516:750–768.

Crummy, J., Fabian, A. C., Gallo, L., and Ross, R. R. (2006). An explanation for the soft X-ray excess in active galactic nuclei. *MNRAS*, 365:1067–1081.

den Herder, J. W., Brinkman, A. C., Kahn, S. M., Branduardi-Raymont, G., Thomsen, K., Aarts, H., Audard, M., Bixler, J. V., den Boggende, A. J., Cottam, J., Decker, T., Dubbeldam, L., Erd, C., Goulooze, H., Güdel, M., Guttridge, P., Hailey, C. J., Janabi, K. A., Kaastra, J. S., de Korte, P. A. J., van Leeuwen, B. J., Mauche, C., McCalden, A. J., Mewe, R., Naber, A., Paerels, F. B., Peterson, J. R., Rasmussen, A. P., Rees, K., Sakelliou, I., Sako, M., Spodek, J., Stern, M., Tamura, T., Tandy, J., de Vries, C. P., Welch, S., and Zehnder, A. (2001). The Reflection Grating Spectrometer on board XMM-Newton. *A&A*, 365:L7–L17.

Diehl, R., Halloin, H., Kretschmer, K., Lichti, G. G., Schönfelder, V., Strong, A. W., von Kienlin, A., Wang, W., Jean, P., Knödlseder, J., Roques, J.-P., Weidenspointner, G., Schanne, S., Hartmann, D. H., Winkler, C., and Wunderer, C. (2006). Radioactive ^{26}Al from massive stars in the Galaxy. *Nature*, 439:45–47.

Done, C., Davis, S. W., Jin, C., Blaes, O., and Ward, M. (2012). Intrinsic disc emission and the soft X-ray excess in active galactic nuclei. *MNRAS*, 420:1848–1860.

Espaillat, C., Bregman, J., Hughes, P., and Lloyd-Davies, E. (2008). Wavelet analysis of agn x-ray time series: A qpo in 3c 273? *The Astrophysical Journal*, 679(1):182.

Fang, T., Marshall, H. L., Lee, J. C., Davis, D. S., and Canizares, C. R. (2002). Chandra Detection of O VIII Lyα Absorption from an Overdense Region in the Intergalactic Medium. *ApJ*, 572:L127–L130.

Fang, T., Sembach, K. R., and Canizares, C. R. (2003). Chandra Detection of Local O VII Heα Absorption along the Sight Line toward 3C 273. *ApJ*, 586:L49–L52.

Ferrarese, L. and Merritt, D. (2000). A Fundamental Relation between Supermassive Black Holes and Their Host Galaxies. *ApJ*, 539:L9–L12.

Fraternali, F. and Tomassetti, M. (2012). Estimating gas accretion in disc galaxies using the Kennicutt-Schmidt law. *MNRAS*, 426:2166–2177.

Fukumura, K., Kazanas, D., Contopoulos, I., and Behar, E. (2010). Magnetohydrodynamic accretion disk winds as x-ray absorbers in active galactic nuclei. *The Astrophysical Journal*, 715(1):636.

Gabriel, A. H. and Jordan, C. (1969). Long Wavelength Satellites to the He-like Ion Resonance Lines in the Laboratory and in the Sun. *Nature*, 221:947–949.

Gierliński, M. and Done, C. (2004). Is the soft excess in active galactic nuclei real? *MNRAS*, 349:L7–L11.

Grandi, P., Guainazzi, M., Mineo, T., Parmar, A. N., Fiore, F., Matteuzzi, A., Nicastro, F., Perola, G. C., Piro, L., Cappi, M., Cusumano, G., Frontera, S., Giarrusso, F., Palazzi, E., and Piraino, S. (1997). BeppoSAX observation of 3C 273: broadband spectrum and detection of a low-energy absorption feature. *A&A*, 325:L17–L20.

Greenstein, J. L. and Schmidt, M. (1964). The Quasi-Stellar Radio Sources 3C 48 and 3C 273. *ApJ*, 140:1.

Haardt, F. and Maraschi, L. (1993). X-ray spectra from two-phase accretion disks. *ApJ*, 413:507–517.

Harris, D. E. and Stern, C. P. (1987). X-ray emission associated with the jet in 3C 273. *ApJ*, 313:136–140.

Henry, J. P., Becklin, E. E., and Telesco, C. M. (1984). Infrared observations of the 3C 273 jet. *ApJ*, 280:98–101.

Jansen, F., Lumb, D., Altieri, B., Clavel, J., Ehle, M., Erd, C., Gabriel, C., Guainazzi, M., Gondoin, P., Much, R., Munoz, R., Santos, M., Schartel, N., Texier, D., and Vacanti, G. (2001). XMM-Newton observatory. I. The spacecraft and operations. *A&A*, 365:L1–L6.

Jester, S., Harris, D. E., Marshall, H. L., and Meisenheimer, K. (2006). New Chandra Observations of the Jet in 3C 273. I. Softer X-Ray than Radio Spectra and the X-Ray Emission Mechanism. *ApJ*, 648:900–909.

Johnston, K. J., Fey, A. L., Zacharias, N., Russell, J. L., Ma, C., de Vegt, C., Reynolds, J. E., Jauncey, D. L., Archinal, B. A., Carter, M. S., Corbin, T. E., Eubanks, T. M., Florkowski, D. R., Hall, D. M., McCarthy, D. D., McCulloch, P. M., King, E. A., Nicolson, G., and Shaffer, D. B. (1995). A Radio Reference Frame. *AJ*, 110:880.

Jovanović, P. and Popović, L. Č. (2009). X-ray Emission From Accretion Disks of AGN: Signatures of Supermassive Black Holes. *ArXiv e-prints*.

Kaastra, J. S. and Barr, P. (1989). Soft and hard X-ray variability from the accretion disk of NGC 5548. *A&A*, 226:59–68.

Kaastra, J. S., Mewe, R., and Nieuwenhuijzen, H. (1996). SPEX: a new code for spectral analysis of X & UV spectra. In Yamashita, K. and Watanabe, T., editors, *UV and X-ray Spectroscopy of Astrophysical and Laboratory Plasmas*, pages 411–414.

Kellogg, E., Gursky, H., Leong, C., Schreier, E., Tananbaum, H., and Giacconi, R. (1971). X-Ray Observations of the Virgo Cluster, NGC 5128, and 3c 273 from the UHURU Satellite. *ApJ*, 165:L49.

Krolik, J. H. and Kriss, G. A. (2001). Warm absorbers in active galactic nuclei: A multitemperature wind. *The Astrophysical Journal*, 561(2):684.

Lynden-Bell, D. (1969). Galactic Nuclei as Collapsed Old Quasars. *Nature*, 223:690–694.

Magdziarz, P., Blaes, O. M., Zdziarski, A. A., Johnson, W. N., and Smith, D. A. (1998). A spectral decomposition of the variable optical, ultraviolet and X-ray continuum of NGC 5548. *MNRAS*, 301:179–192.

Marasco, A., Marinacci, F., and Fraternali, F. (2013). On the origin of the warm–hot absorbers in the milky way's halo. *Monthly Notices of the Royal Astronomical Society*, 433(2):1634–1647.

Mathur, S., Weinberg, D. H., and Chen, X. (2003). X-ray Observations of the Warm-Hot Intergalactic Medium. In Rosenberg, J. L. and Putman, M. E., editors, *The IGM/Galaxy Connection. The Distribution of Baryons at z=0*, volume 281 of *Astrophysics and Space Science Library*, page 103.

Mehdipour, M., Kaastra, J. S., Kriss, G. A., Cappi, M., Petrucci, P. O., Steenbrugge, K. C., Arav, N., Behar, E., Bianchi, S., Boissay, R., Branduardi-Raymont, G., Costantini, E., Ebrero, J., Di Gesu, L., Harrison, F. A., Kaspi, S., De Marco, B., Matt, G., Paltani, S., Peterson, B. M., Ponti, G., Pozo Nuñez, F., De Rosa, A., Ursini, F., de

Vries, C. P., Walton, D. J., and Whewell, M. (2015a). Anatomy of the AGN in NGC 5548. I. A global model for the broadband spectral energy distribution. *A&A*, 575:A22.

Mehdipour, M., Kaastra, J. S., Kriss, G. A., Cappi, M., Petrucci, P. O., Steenbrugge, K. C., Arav, N., Behar, E., Bianchi, S., Boissay, R., Branduardi-Raymont, G., Costantini, E., Ebrero, J., Di Gesu, L., Harrison, F. A., Kaspi, S., De Marco, B., Matt, G., Paltani, S., Peterson, B. M., Ponti, G., Pozo Nuñez, F., De Rosa, A., Ursini, F., de Vries, C. P., Walton, D. J., and Whewell, M. (2015b). Anatomy of the AGN in NGC 5548. I. A global model for the broadband spectral energy distribution. *A&A*, 575.

Middleton, M., Done, C., Ward, M., Gierliński, M., and Schurch, N. (2009). RE J1034+396: the origin of the soft X-ray excess and quasi-periodic oscillation. *MNRAS*, 394:250–260.

Miller, M. J., Hodges-Kluck, E. J., and Bregman, J. N. (2016). The Milky Way's Hot Gas Kinematics: Signatures in Current and Future OVII Absorption Line Observations. *ApJ*, 818:112.

Mitsuda, K., Bautz, M., Inoue, H., Kelley, R. L., Koyama, K., Kunieda, H., Makishima, K., Ogawara, Y., Petre, R., Takahashi, T., Tsunemi, H., White, N. E., Anabuki, N., Angelini, L., Arnaud, K., Awaki, H., Bamba, A., Boyce, K., Brown, G. V., Chan, K.-W., Cottam, J., Dotani, T., Doty, J., Ebisawa, K., Ezoe, Y., Fabian, A. C., Figueroa, E., Fujimoto, R., Fukazawa, Y., Furusho, T., Furuzawa, A., Gendreau, K., Griffiths, R. E., Haba, Y., Hamaguchi, K., Harrus, I., Hasinger, G., Hatsukade, I., Hayashida, K., Henry, P. J., Hiraga, J. S., Holt, S. S., Hornschemeier, A., Hughes, J. P., Hwang, U., Ishida, M., Ishisaki, Y., Isobe, N., Itoh, M., Iyomoto, N., Kahn, S. M., Kamae, T., Katagiri, H., Kataoka, J., Katayama, H., Kawai, N., Kilbourne, C., Kinugasa, K., Kissel, S., Kitamoto, S., Kohama, M., Kohmura, T., Kokubun, M., Kotani, T., Kotoku, J., Kubota, A., Madejski, G. M., Maeda, Y., Makino, F., Markowitz, A., Matsumoto, C., Matsumoto, H., Matsuoka, M., Matsushita, K., McCammon, D., Mihara, T., Misaki, K., Miyata, E., Mizuno, T., Mori, K., Mori, H., Morii, M., Moseley, H., Mukai, K., Murakami, H., Murakami, T., Mushotzky, R., Nagase, F., Namiki, M., Negoro, H., Nakazawa, K., Nousek, J. A., Okajima, T., Ogasaka, Y., Ohashi, T., Oshima, T., Ota, N., Ozaki, M., Ozawa, H., Parmar, A. N., Pence, W. D., Porter, F. S., Reeves, J. N., Ricker, G. R., Sakurai, I., Sanders, W. T., Senda, A., Serlemitsos, P., Shibata, R., Soong, Y., Smith, R., Suzuki, M., Szymkowiak, A. E., Takahashi, H., Tamagawa, T., Tamura, K., Tamura, T., Tanaka, Y., Tashiro, M., Tawara, Y., Terada, Y., Terashima, Y., Tomida, H., Torii, K., Tsuboi, Y., Tsujimoto, M., Tsuru, T. G., Turner, M. J. L. ., Ueda, Y., Ueno, S., Ueno, M., Uno, S., Urata, Y., Watanabe, S., Yamamoto, N., Yamaoka, K., Yamasaki, N. Y., Yamashita, K., Yamauchi, M., Yamauchi, S., Yaqoob, T., Yonetoku, D., and Yoshida, A. (2007). The X-Ray Observatory Suzaku. *PASJ*, 59:S1–S7.

Nakanishi, H. and Sofue, Y. (2003). Three-dimensional distribution of the ism in the milky way galaxy: I. the h i disk. *Publications of the Astronomical Society of Japan*, 55(1):191–202.

Paltani, S. and Türler, M. (2003). Dynamics of the Lyα and C IV Emitting Gas in 3C 273. *ApJ*, 583:659–669.

Paltani, S. and Türler, M. (2005). The mass of the black hole in 3C 273. *A&A*, 435:811–820.

Perry, J. J., Ward, M. J., and Jones, M. (1987). 3C 273 and the power-law myth. *MNRAS*, 228:623–634.

Piconcelli, E., Jimenez-Bailón, E., Guainazzi, M., Schartel, N., Rodríguez-Pascual, P. M., and Santos-Lleó, M. (2005). The XMM-Newton view of PG quasars. I. X-ray continuum and absorption. *A&A*, 432:15–30.

Porquet, D., Mewe, R., Dubau, J., Raassen, A. J. J., and Kaastra, J. S. (2001). Line ratios for helium-like ions: Applications to collision-dominated plasmas. *A&A*, 376:1113–1122.

Pradhan, A. K. and Nahar, S. N. (2011). *Atomic Astrophysics and Spectroscopy*. Cambridge University Press.

Proga, D., Stone, J. M., and Kallman, T. R. (2000). Dynamics of line-driven disk winds in active galactic nuclei. *The Astrophysical Journal*, 543(2):686.

Rix, H.-W. and Bovy, J. (2013). The Milky Way's stellar disk. Mapping and modeling the Galactic disk. *A&A Rev.*, 21:61.

Röser, H.-J., Meisenheimer, K., Neumann, M., Conway, R. G., and Perley, R. A. (2000). The jet of 3C 273 observed with ROSAT HRI. *A&A*, 360:99–106.

Rybicki, G. B. and Lightman, A. P. (1979). *Radiative processes in astrophysics*.

Sambruna, R. M., Urry, C. M., Tavecchio, F., Maraschi, L., Scarpa, R., Chartas, G., and Muxlow, T. (2001). Chandra Observations of the X-Ray Jet of 3C 273. *ApJ*, 549:L161–L165.

Schmidt, M. (1963). 3C 273 : A Star-Like Object with Large Red-Shift. *Nature*, 197:1040.

Sembach, K. (2001). Pierce Prize Lecture: High Velocity Clouds: Cosmological and Galactic Weather. In *American Astronomical Society Meeting Abstracts*, volume 33 of *Bulletin of the American Astronomical Society*, page 1478.

Silk, J. and Rees, M. J. (1998). Quasars and galaxy formation. *A&A*, 331:L1–L4.

Soldi, S., Türler, M., Paltani, S., Aller, H. D., Aller, M. F., Burki, G., Chernyakova, M., Lähteenmäki, A., McHardy, I. M., Robson, E. I., Staubert, R., Tornikoski, M., Walter, R., and Courvoisier, T. J.-L. (2008). The multiwavelength variability of 3C 273. *A&A*, 486:411–425.

Steenbrugge, K. C., Kaastra, J. S., Crenshaw, D. M., Kraemer, S. B., Arav, N., George, I. M., Liedahl, D. A., van der Meer, R. L. J., Paerels, F. B. S., Turner, T. J., and Yaqoob, T. (2005). Simultaneous X-ray and UV spectroscopy of the Seyfert galaxy NGC 5548. II. Physical conditions in the X-ray absorber. *A&A*, 434:569–584.

Strauss, M. A., Huchra, J. P., Davis, M., Yahil, A., Fisher, K. B., and Tonry, J. (1992). A redshift survey of IRAS galaxies. VII - The infrared and redshift data for the 1.936 Jansky sample. *ApJS*, 83:29–63.

Strüder, L., Briel, U., Dennerl, K., Hartmann, R., Kendziorra, E., Meidinger, N., Pfeffermann, E., Reppin, C., Aschenbach, B., Bornemann, W., Bräuninger, H., Burkert, W., Elender, M., Freyberg, M., Haberl, F., Hartner, G., Heuschmann, F., Hippmann, H., Kastelic, E., Kemmer, S., Kettenring, G., Kink, W., Krause, N., Müller, S., Oppitz, A., Pietsch, W., Popp, M., Predehl, P., Read, A., Stephan, K. H., Stötter, D., Trümper, J., Holl, P., Kemmer, J., Soltau, H., Stötter, R., Weber, U., Weichert, U., von Zanthier, C., Carathanassis, D., Lutz, G., Richter, R. H., Solc, P., Böttcher, H., Kuster, M., Staubert, R., Abbey, A., Holland, A., Turner, M., Balasini, M., Bignami, G. F., La Palombara, N., Villa, G., Buttler, W., Gianini, F., Lainé, R., Lumb, D., and Dhez, P. (2001). The European Photon Imaging Camera on XMM-Newton: The pn-CCD camera. *A&A*, 365:L18–L26.

Sunyaev, R. A. and Titarchuk, L. G. (1980). Comptonization of X-rays in plasma clouds - Typical radiation spectra. *A&A*, 86:121–138.

Turner, M. J. L., Abbey, A., Arnaud, M., Balasini, M., Barbera, M., Belsole, E., Bennie, P. J., Bernard, J. P., Bignami, G. F., Boer, M., Briel, U., Butler, I., Cara, C., Chabaud, C., Cole, R., Collura, A., Conte, M., Cros, A., Denby, M., Dhez, P., Di Coco, G., Dowson, J., Ferrando, P., Ghizzardi, S., Gianotti, F., Goodall, C. V., Gretton, L., Griffiths, R. G., Hainaut, O., Hochedez, J. F., Holland, A. D., Jourdain, E., Kendziorra, E., Lagostina, A., Laine, R., La Palombara, N., Lortholary, M., Lumb, D., Marty, P., Molendi, S., Pigot, C., Poindron, E., Pounds, K. A., Reeves, J. N., Reppin, C., Rothenflug, R., Salvetat, P., Sauvageot, J. L., Schmitt, D., Sembay, S., Short, A. D. T., Spragg, J., Stephen, J., Strüder, L., Tiengo, A., Trifoglio, M., Trümper, J., Vercellone, S., Vigroux, L., Villa, G., Ward, M. J., Whitehead, S., and Zonca, E. (2001). The European Photon Imaging Camera on XMM-Newton: The MOS cameras : The MOS cameras. *A&A*, 365:L27–L35.

Uchiyama, Y., Urry, C. M., Cheung, C. C., Jester, S., Van Duyne, J., Coppi, P., Sambruna, R. M., Takahashi, T., Tavecchio, F., and Maraschi, L. (2006). Shedding New Light on the 3C 273 Jet with the Spitzer Space Telescope. *ApJ*, 648:910–921.

Véron-Cetty, M.-P. and Véron, P. (2006). A catalogue of quasars and active nuclei: 12th edition. *A&A*, 455:773–777.

Wang, Q. D. (2009). Global Hot Gas in and around the Galaxy. In Smith, R. K., Snowden, S. L., and Kuntz, K. D., editors, *American Institute of Physics Conference Series*, volume 1156 of *American Institute of Physics Conference Series*, pages 257–267.

Wang, Q. D., Yao, Y., Tripp, T. M., Fang, T.-T., Cui, W., Nicastro, F., Mathur, S., Williams, R. J., Song, L., and Croft, R. (2005). Warm-Hot Gas in and around the Milky Way: Detection and Implications of O VII Absorption toward LMC X-3. *ApJ*, 635:386–395.

Willingale, R., Starling, R. L. C., Beardmore, A. P., Tanvir, N. R., and O'Brien, P. T. (2013). Calibration of X-ray absorption in our Galaxy. *MNRAS*, 431:394–404.

Yao, Y. and Wang, Q. D. (2007). The Galactic Central Diffuse X-Ray Enhancement: A Differential Absorption/Emission Analysis. *ApJ*, 666:242–246.